

# An Impulsive Approach to State Estimation for Multi-Rate Singularly Perturbed Complex Networks Under Bit Rate Constraints

Yuru Guo, Zidong Wang, *Fellow, IEEE*, Jun-Yi Li, *Member, IEEE* and Yong Xu, *Member, IEEE*

**Abstract**—In this paper, the problem of ultimately bounded state estimation is investigated for discrete-time multi-rate singularly perturbed complex networks under the bit rate constraints, where the sensor sampling period is allowed to differ from the updating period of the networks. The facilitation of communication between sensors and the remote estimator through wireless networks, which are subject to bit rate constraints, involves the use of a coding-decoding mechanism. For efficient estimation in the presence of periodic measurements, a specialized impulsive estimation method is developed, which aims to carry out impulsive corrections precisely at the instants when the measurement signal is received by the estimator. By employing the iteration analysis method under the impulsive mechanism, a sufficient condition is established that ensures the exponential boundedness of the estimation error dynamics. Furthermore, an optimization algorithm is introduced for addressing the challenges related to bit rate allocation and the design of desired estimator gains. Within the presented theoretical framework, the correlation between estimation performance and bit rate allocation is elucidated. Finally, a simulation example is provided to demonstrate the validity of the proposed estimation approach.

**Index Terms**—Singularly perturbed systems, multi-rate complex networks, impulsive estimation, constrained bit rate, bit rate allocation.

## I. INTRODUCTION

Complex networks (CNs) are defined as intricate systems composed of numerous nodes connected by edges, which represent the relationships, interactions, or connections between them. The inherent complexity of CNs is a result of the complex coupling among the multitude of network nodes. Over the past decade, various models of CNs, such

This work was supported in part by Key Area Research and Development Program of Guangdong Province under Grant 2021B0101410005, the Natural Science Foundation of Guangdong Province of China under Grants 2021A1515011634 and 2021B1515420008, the National Natural Science Foundation of China under Grants U22A2044 and 62206063, the Local Innovative and Research Teams Project of Guangdong Special Support Program of China under Grant 2019BT02X353, and the China Scholarship Council under Grant 202208440312. (*Corresponding author: Jun-Yi Li*)

Yuru Guo and Yong Xu are with the Guangdong-Hong Kong Joint Laboratory for Intelligent Decision and Cooperative Control, Guangdong Provincial Key Laboratory of Intelligent Decision and Cooperative Control, School of Automation, Guangdong University of Technology, Guangzhou 510006, China. (E-mails: guo\_yuru0626@163.com; yxu@gdut.edu.cn)

Zidong Wang is with the Department of Computer Science, Brunel University London, Uxbridge UB8 3PH, United Kingdom. (E-mail: Zidong.Wang@brunel.ac.uk)

Jun-Yi Li is with the Guangdong-Hong Kong Joint Laboratory for Intelligent Decision and Cooperative Control, Guangdong Provincial Key Laboratory of Intelligent Decision and Cooperative Control, School of Automation, Guangdong University of Technology, Guangzhou 510006, China, and also with the Project Team of Intelligent Unmanned Surface Vessels for Waste Collection, Pazhou Lab, Guangzhou 510330, China. (E-mail: jun-yi-li@foxmail.com)

as switching CNs [48], time-varying CNs [47], time-delayed CNs [9], and CNs with incomplete measurements [46], have garnered widespread attention within research communities. Based on these models, substantial advancements have been achieved in areas such as state estimation, stability, synchronization control, and other dynamics analysis problems [4], [6]. Furthermore, CNs are applied in a variety of practical scenarios including social networks, transportation networks, power grids, computer networks and biological networks [8], [13], [19], [22].

The prevailing literature commonly presupposes that the states of CNs evolve uniformly on the same time scale, but this might not be true for specific CNs, where the presence of differing time scales is a notable characteristic. In fact, as a unique category of CNs, the so-called singularly perturbed complex networks (SPCNs) are distinguished by their complex dynamics and structures. The singularly perturbed parameter (SPP) plays a crucial role in defining these multiple time scales. It typically represents a small parameter that separates the fast and slow dynamics within the system. By introducing the SPP, one can model systems where certain states or processes evolve much more rapidly than others [23], [32], [36]. In recent years, considerable interest has been devoted to the study of SPCNs due to their extensive applications in various practical domains, such as power grids, robots and vehicles systems. Moreover, SPCNs have been applied in state estimation and synchronization control problems [20], [25], [26]. These investigations lay the groundwork for ongoing research into SPCNs, particularly in relation to diverse phenomena.

Current research on SPCNs commonly assumes that network and sensor measurements are sampled at uniform rates. Unfortunately, this assumption often does not reflect practical scenarios, as different system components typically have distinct sampling periods due to their varied physical properties. For instance, in certain industrial processes such as aluminum electrolysis, where the system state changes slowly, there is no pressing need to sample measurements synchronously with every state update [29], [30], [38]. On the other hand, in scenarios like wireless transmission channels, which are characterized by limited network resources, intermittent sampling and transmission of sensor data become crucial for conserving network resources. The significance of *multi-rate* CNs lies in the fact that they are common and crucial in practical applications. They can more accurately capture the dynamic characteristics of various parts of a system, allowing for optimized resource utilization and improved system efficiency [7], [11], [12], [28], [52].

In real-world applications, accurately capturing the internal states of CNs is challenging due to factors like measurement errors and sensor noises, and this highlights the need for effective state estimation strategies especially for dynamic analysis tasks in multi-rate systems, see some recent studies [5], [10], [45], [51]. The lifting technique has been applied to multi-rate systems to develop estimation algorithms by constructing state equations at each measurement sampling point [34], [37], [49]. Furthermore, the use of switching concepts and impulsive structures in estimators for multi-rate systems has been explored in [2], [3], [14], [50]. However, the specific challenge of estimating multi-rate SPCNs using these methods remains an area that needs further research.

The rapid advancements in digital network technology have triggered a significant change in communication mechanisms within control systems [1], [18]. Traditional analog communication methods are increasingly seen as insufficient for the needs of modern control systems, leading to the rise of digital communication strategies as a more suitable alternative [35]. However, digital networks often face inherent bandwidth constraints, which can cause issues like signal fading and packet dropouts during wireless transmission [16], [39]. A key aspect lies in the consideration of bit rate, a parameter delineating the volume of data transmissible in a given unit of time over a digital network. This rate is crucial for defining the communication bandwidth. However, due to limited bandwidth resources, the bit rate is often restricted, posing challenges for ensuring fast and reliable data transmission in wireless digital networks [27], [33], [40]. Therefore, effectively allocating the bit rate to each node to prevent data collision becomes a critical concern in managing these networks [15].

Recently, scholarly attention has been directed towards investigating the dynamics of systems operating under constrained bit rates. Notably, the work [17] delves into the realm of distributed filtering in wireless sensor networks, particularly when confronted with limited bit rates, where a novel bit rate allocation protocol is introduced to address these challenges. In [24], the investigation centers on the stabilization problem of an event-triggered system operating within the constraints of a bit-rate constrained network, where the analysis encompasses considerations for both bounded transmission delay and Markov feedback dropout. It is important to note, however, that most existing studies focus primarily on common networked systems with limited bit rates. In contrast, the bit-rate-constrained estimation problem in multi-rate SPCNs has not received adequate attention despite its practical relevance. This lack of research underscores a significant gap and highlights the need for further investigation into this specific area, particularly to address the unique challenges presented by multi-rate SPCNs.

Derived from the aforementioned discourse, our investigation revolves around the following three key challenges.

- 1) *Modeling Multi-Rate SPCNs*: Developing a model that captures the impact of bit rate constraints on multi-rate SPCNs, addressing the practical limitations imposed by transmission channel capacities.
- 2) *Novel Estimation Method Design*: Creating an estimation method tailored for multi-rate SPCNs, which utilizes intermittent measurement reception to accommodate varied data collection and transmission frequencies.

- 3) *Optimizing Estimator Gain and Bit Rates*: Designing estimator gains to align with impulsive characteristics under bit rate limitations, while simultaneously optimizing bit rate allocation and gain co-design to enhance network performance.

Addressing these challenges is essential to improve state estimation in multi-rate SPCNs, which is crucial for their reliability and efficiency in practical scenarios. In response to the identified challenges, the main contributions of this paper are highlighted as follows.

- 1) *Model construction*. For the first time, the constrained bit rate is incorporated into the modeling of discrete-time multi-rate SPCNs. A coding-decoding model is established, focusing on the fast and slow states of the networks, thereby providing a more realistic representation of these systems under bit rate constraints.
- 2) *Estimate method design*. An impulsive estimation method is devised, which capitalizes on the periodic transmission nature of the sensor network. Compared with the existing methods [21], [50], this method involves executing impulse updates at the moments when measurements are received by the estimator, avoiding the conversion from a multi-rate system to a single-rate system.
- 3) *Gain design and optimization*. The interaction between estimation performance, bit rate, and sampling period is analyzed under the impulse mechanism. To enhance network performance, a co-optimization algorithm is introduced. This algorithm is aimed at optimizing the allocation of bit rates and designing the gains for the impulsive estimator, striking a balance between effective data transmission and accurate state estimation.

This paper is divided into five parts, which are organized as follows. Section II provides a comprehensive description of multi-rate SPCNs, including details on the coding-decoding process under bit-rate constraints, the structure of the adopted impulsive estimator, and an overview of the impulsive error dynamics. Section III presents the main boundedness analysis results, the methodology for designing estimator gains, as well as the collaborative approach for co-designing bit-rate allocation and estimator gains. In Section IV, a numerical example is provided, along with explanatory notes, to validate the correctness of the derived theoretical results. Section V draws the conclusion.

*Notations*: Throughout this article, we define the representation of some symbols.  $\mathbb{R}^m$ ,  $\mathbb{R}^{m \times n}$ , and  $\mathbb{N}^+$  represent the  $m$ -dimensional Euclidean space, the  $m \times n$  real matrices, and the positive integers, respectively. The symbol  $\|\cdot\|$  refers to the Euclidean norm, and  $|\cdot|$  stands for the absolute value. For a matrix  $X$ , its transpose is denoted by  $X^T$ , and  $\lambda_{\min}(X)$  signifies its minimum eigenvalue. An  $n$ -elements column vector is expressed by  $\text{col}_n$ . The diagonal matrix is articulated as  $\text{diag}\{\dots\}$ . The Kronecker product is represented by the symbol  $\otimes$ .

## II. PROBLEM FORMULATION

### A. Multi-Rate Singularly Perturbed Complex Networks

Consider a class of multi-rate SPCNs of the following form:

$$x_i(p_t) = A_\varepsilon x_i(p_{t-1}) + \tilde{J}_\varepsilon(x_i(p_{t-1}))$$

$$+ H_i \vartheta(p_{t-1}) + \sum_{j=1}^N \omega_{ij} \Gamma_\varepsilon x_j(p_{t-1}) \quad (1)$$

with

$$\begin{aligned} x_i(p_t) &\triangleq \begin{bmatrix} x_{if}(p_t) \\ x_{is}(p_t) \end{bmatrix}, \quad H_i \triangleq \begin{bmatrix} H_{i1} \\ H_{i2} \end{bmatrix}, \\ A_\varepsilon &\triangleq \begin{bmatrix} A_1 & A_2 \\ \varepsilon A_3 & \varepsilon A_4 \end{bmatrix}, \quad \Gamma_\varepsilon \triangleq \begin{bmatrix} \Gamma_1 & \Gamma_2 \\ \varepsilon \Gamma_3 & \varepsilon \Gamma_4 \end{bmatrix}, \\ \tilde{J}_\varepsilon(x_i(p_t)) &\triangleq \begin{bmatrix} \tilde{g}(x_{if}(p_t)) + D x_{is}(p_t) \\ \varepsilon (\tilde{h}(x_{is}(p_t)) + F x_{is}(p_t)) \end{bmatrix}. \end{aligned}$$

Here,  $i$  represents the node number, defined as  $i \in \mathcal{N} \triangleq [1, 2, \dots, N]$ ; the state of SPCNs denoted by  $x_i(p_t) \in \mathbb{R}^n$ , encompasses both the fast state  $x_{if}(p_t) \in \mathbb{R}^{n_f}$  and the slow state  $x_{is}(p_t) \in \mathbb{R}^{n_s}$  with  $n_f + n_s = n$ ; the variable  $p_t$  (with  $t \in \mathbb{N}^+$ ) represents the  $t$ -th updating instant of the state, and the state update period of SPCNs is indicated by  $\hbar \triangleq p_t - p_{t-1}$ ;  $\varepsilon$  serves as a small positive constant governing the separation of the fast and slow time scales; the external disturbance  $\vartheta(p_t) \in \mathbb{R}^c$  adheres to the constraint  $\|\vartheta(p_t)\| \leq \vartheta_0$ ;  $\tilde{g}(\cdot)$  and  $\tilde{h}(\cdot)$  are the nonlinear functions that will be introduced later.

In (1),  $A_\varepsilon$  is a parameter matrix characterized by its components, namely  $A_1 \in \mathbb{R}^{n_f \times n_f}$ ,  $A_2 \in \mathbb{R}^{n_f \times n_s}$ ,  $A_3 \in \mathbb{R}^{n_s \times n_f}$ , and  $A_4 \in \mathbb{R}^{n_s \times n_s}$ ; the coupled configuration matrix  $W = \omega_{ij} \in \mathbb{R}^{n \times n}$  adheres to the constraint  $\sum_{j=1}^N \omega_{ij} = 0$  for each  $i \in \mathcal{N}$ , signifying that node  $i$  can receive information from node  $j$  if  $\omega_{ij} > 0$ , otherwise,  $\omega_{ij} = 0$ ; the inner coupling matrix  $\Gamma_\varepsilon$  defines the relationships among the various components within a node, delineated by  $\Gamma_1 \in \mathbb{R}^{n_f \times n_f}$ ,  $\Gamma_2 \in \mathbb{R}^{n_f \times n_s}$ ,  $\Gamma_3 \in \mathbb{R}^{n_s \times n_f}$ , and  $\Gamma_4 \in \mathbb{R}^{n_s \times n_s}$ ; additionally,  $D \in \mathbb{R}^{n_f \times n_s}$ ,  $F \in \mathbb{R}^{n_s \times n_s}$ ,  $H_{i1} \in \mathbb{R}^{n_f \times c}$ , and  $H_{i2} \in \mathbb{R}^{n_s \times c}$  are some constant matrices.

The nonlinear functions  $\tilde{g}(\cdot) \in \mathbb{R}^{n_f}$  and  $\tilde{h}(\cdot) \in \mathbb{R}^{n_s}$  satisfy [31]

$$\begin{aligned} &(\tilde{g}(\acute{a}) - \tilde{g}(\grave{a}) - \tilde{\psi}_1(\acute{a} - \grave{a}))^T \\ &\quad \times (\tilde{g}(\acute{a}) - \tilde{g}(\grave{a}) - \tilde{\psi}_2(\acute{a} - \grave{a})) \leq 0, \quad (2) \end{aligned}$$

$$\begin{aligned} &(\tilde{h}(\acute{c}) - \tilde{h}(\grave{c}) - \tilde{\chi}_1(\acute{c} - \grave{c}))^T \\ &\quad \times (\tilde{h}(\acute{c}) - \tilde{h}(\grave{c}) - \tilde{\chi}_2(\acute{c} - \grave{c})) \leq 0 \quad (3) \end{aligned}$$

where  $\acute{a}, \grave{a} \in \mathbb{R}^{n_f}$  and  $\acute{c}, \grave{c} \in \mathbb{R}^{n_s}$  are some vectors, and  $\tilde{\psi}_i \in \mathbb{R}^{n_f \times n_f}$  and  $\tilde{\chi}_i \in \mathbb{R}^{n_s \times n_s}$  ( $i \in \{1, 2\}$ ) are known matrices.

In this paper, we are concerned with multi-rate SPCNs whose sensor sampling frequency is lower than the state update frequency, where the measurement output is represented by

$$y_i(k_m) = C_i x_i(k_m) + M_i \vartheta(k_m), \quad i \in \mathcal{N} \quad (4)$$

with

$$y_i(k_m) \triangleq \begin{bmatrix} y_{if}(k_m) \\ y_{is}(k_m) \end{bmatrix}, \quad M_i \triangleq \begin{bmatrix} M_{i1} \\ M_{i2} \end{bmatrix}, \quad C_i \triangleq \text{diag}\{C_{if}, C_{is}\}.$$

Here,  $k_m$  ( $m \in \mathbb{N}^+$ ) is the sampling instant of sensors, and  $b\hbar \triangleq k_m - k_{m-1}$  signifies the sampling period with a known integer  $b > 1$ ;  $M_{i1}$ ,  $M_{i2}$ ,  $C_{if}$  and  $C_{is}$  are known constant matrices;  $y_i(k_m) \in \mathbb{R}^v$  consisting of  $y_{if}(k_m) \in \mathbb{R}^{v_f}$  and  $y_{is}(k_m) \in \mathbb{R}^{v_s}$  ( $v_f + v_s = v$ ) denotes the measurement output. Without loss of generality, we assume that 1) the state update

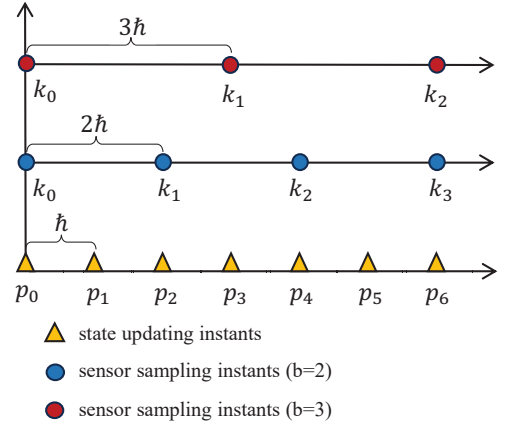


Fig. 1. Schematic diagram of the multi-rate sampling mechanism.

period  $\hbar$  is a fixed constant, and 2) the initial updating instants of state and the initial sampling instants of sensor are equal (i.e.  $p_0 = k_0$ ). Fig. 1 illustrates the state updating and sensor sampling rules with different integer  $b$ .

### B. Data Transmission Under Constrained Bit Rate

The available bandwidth in wireless networks is commonly limited, imposing constraints on sustained high-speed data transmission. Consequently, the bit rate, representing the quantity of data transmitted per unit of time through the channel, is inherently restricted. This limitation underscores the necessity for judicious resource allocation, given that all sensors are constrained in the number of bits available for data transmission at sampling instants  $k_m$ . Hence, it becomes essential to allocate appropriate bits to each sensor, aiming to prevent data collisions during wireless transmission. Sensor  $i$  is assigned bit rate denoted by  $B_i$  (a positive integer), and the subsequent expression delineates this allocation [17],

$$B \geq \sum_{i=1}^N B_i \quad (5)$$

where  $B$  is the available bit rate of the entire communication network.

To enhance the transmission of sensor data within the confines of a bandwidth-limited channel, the implementation of data compression becomes imperative. This can be effectively accomplished through a uniform quantizer. With a scalar  $\sigma_i > 0$ , determined by the sensor's range, the quantization region of the  $i$ -th sensor node is characterized by

$$|y_i^{(j)}(k_m)| \leq \sigma_i, \quad j \in [1, 2, \dots, v] \quad (6)$$

where  $y_i^{(j)}(k_m)$  represents the  $j$ -th element of the measurement  $y_i(k_m)$ .

Upon selecting a quantization level  $q_i$  for sensor node  $i$ , the quantization region can be uniformly divided into sub-hyperrectangles. Subsequently, the ranges of these sub-hyperrectangles are designated by

$$\mathcal{Q}_1^{(i,j)}(\sigma_i) : -\sigma_i \leq y_i^{(j)}(k_m) < -\sigma_i + \frac{2\sigma_i}{q_i}$$

$$\begin{aligned} \mathcal{Q}_2^{(i,j)}(\sigma_i) &: -\sigma_i + \frac{2\sigma_i}{q_i} \leq y_i^{(j)}(k_m) < -\sigma_i + \frac{4\sigma_i}{q_i} \\ &\vdots \\ \mathcal{Q}_{q_i}^{(i,j)}(\sigma_i) &: \sigma_i - \frac{2\sigma_i}{q_i} \leq y_i^{(j)}(k_m) \leq \sigma_i. \end{aligned} \quad (7)$$

The maximum quantization level  $\hat{q}_i$  of sensor node  $i$  is limited by allocated bits, i.e.,

$$\hat{q}_i = \lfloor \sqrt[v]{2^{B_i}} \rfloor \quad (8)$$

where the symbol  $\lfloor \cdot \rfloor$  stands for the rounding down function.

Give the dispersion of sensor measurements within the quantization region defined in (7). Denote the quantization region that each element of sensor node  $i$  is mapped to by the sequence  $\{d_i^{(1)}, \dots, d_i^{(v)}\}$ . In the coder, it employs binary characters, 0 and 1, for encoding the sequence of numbers. Depending on the diverse time scales inherent in SPCNs, the resulting codeword generated by the coder is articulated as  $\mathcal{Y}_i(k_m) \triangleq (\mathcal{Y}_{if}(k_m), \mathcal{Y}_{is}(k_m))$  with  $\mathcal{Y}_{if}(k_m) = \hat{\eta}_i(d_{if}^{(1)}, \dots, d_{if}^{(v)})$  and  $\mathcal{Y}_{is}(k_m) = \hat{\eta}_i(d_{is}^{(v_f+1)}, \dots, d_{is}^{(v)})$ , where  $\hat{\eta}_i(\cdot)$  is the coding function.

In the decoder, the codewords transmitted over the wireless network are decoded to an approximation to the original signal. The central value of sub-hyperrectangle is denoted by

$$\hat{\eta}_i(\mathcal{Y}_i(k_m)) \triangleq [z_i^{(1)} \quad \dots \quad z_i^{(v)}]^T \quad (9)$$

where  $\hat{\eta}_i(\cdot)$  is a decoding function, and the central value is deduced by

$$z_i^{(j)} \triangleq -\sigma_i + \frac{(2d_i^{(j)} - 1)\sigma_i}{\hat{q}_i}, \quad j \in [1, 2, \dots, v].$$

Subsequently, the quantization error of the measurement output is given as

$$\|y_i(k_m) - \hat{\eta}_i(\mathcal{Y}_i(k_m))\| \leq \frac{\sqrt{v}\sigma_i}{\hat{q}_i}. \quad (10)$$

For simplicity, the decoding vector is expressed by the following form:

$$\bar{y}_i(k_m) \triangleq \begin{bmatrix} \bar{y}_{if}(k_m) \\ \bar{y}_{is}(k_m) \end{bmatrix} = \begin{bmatrix} \hat{\eta}_i(\mathcal{Y}_{if}(k_m)) \\ \hat{\eta}_i(\mathcal{Y}_{is}(k_m)) \end{bmatrix} \quad (11)$$

where the decoding error is defined as

$$\delta_i(k_m) \triangleq y_i(k_m) - \bar{y}_i(k_m). \quad (12)$$

*Remark 1:* In wireless communication networks, bit rate allocation can be managed using dynamic or static approaches. Dynamic methods adjust bit rates according to the changing demands of user devices, improving the efficiency of individual data transfers. On the other hand, static methods assign bit rates based on predetermined rules. It particularly suitable for environments where multiple users must share limited bandwidth, promoting fair data distribution. This study adopts a static bit rate allocation approach within SPCNs to maintain consistent and equitable bandwidth distribution across all network nodes.

*Remark 2:* In our study, sensors are assumed to sample and transmit data periodically over a wireless network, a common

practice in bandwidth-limited communication environments. Adopting a periodic sampling strategy helps reduce the volume of data transmission, which in turn mitigates network load and effectively alleviates network congestion. However, this approach inherently involves a trade-off: it may compromise the accuracy of state estimation due to the reduced frequency of sensor measurements. This scenario underscores the need for developing efficient state estimators. Such estimators are crucial to achieve satisfactory estimation performance, balancing the limitations imposed by network bandwidth constraints with the requirement for accurate and reliable state estimation. The challenge lies in designing these estimators to function optimally within the constraints of periodic data transmission while maintaining high estimation accuracy.

### C. Impulsive State Estimator

Based on the insights from Section II-A, we observe that the sensor's sampling rate in SPCNs is slower than the rate at which the system's state updates. This discrepancy implies that the estimator *cannot* perform corrections at every state update instant  $p_t$ . To address this challenge, this paper introduces an innovative impulse-based approach. Within the sensor sampling interval  $(k_{m-1}, k_m]$ , the estimator leverages the system dynamic model and the previous state estimate to predict the state. Subsequently, the estimator performs impulsive update utilizing sensor measurements at the specific sensor sampling instants  $k_m$ . As such, the design of impulsive estimator is divided into two parts. During the interval  $(k_{m-1}, k_m]$ , the estimator is represented by

$$\begin{aligned} \hat{x}_i(p_t) &= A_\varepsilon \hat{x}_i(p_{t-1}) + \tilde{J}_\varepsilon(\hat{x}_i(p_{t-1})) \\ &\quad + \sum_{j=1}^N \omega_{ij} \Gamma_\varepsilon \hat{x}_j(p_{t-1}), \quad p_t \in (k_{m-1}, k_m] \end{aligned} \quad (13)$$

where  $\hat{x}_i(p_t) \triangleq [\hat{x}_{if}^T(p_t) \quad \hat{x}_{is}^T(p_t)]^T$  denotes the state estimate of the node  $i$ .

At the sensor sampling instant  $k_m$  ( $m \in \mathbb{N}^+$ ), the remote estimator successfully receives the measurement. Adhere to the output  $\bar{y}_i(k_m)$  of the decoder, the estimator is constructed as

$$\hat{x}_i^+(k_m) = \hat{x}_i(k_m) + L_i(\bar{y}_i(k_m) - C_i \hat{x}_i(k_m)) \quad (14)$$

where  $\hat{x}_i^+(k_m)$  represents the impulsive update state and  $L_i \triangleq \text{diag}\{L_{if}, L_{is}\}$  denotes the estimator gain to be designed with  $L_{if} \in \mathbb{R}^{n_f \times v_f}$  and  $L_{is} \in \mathbb{R}^{n_s \times v_s}$ .

*Remark 3:* In addressing the state estimation challenges of multi-rate systems, most existing studies utilize methods like the lifting technique [21] and the pseudo measurement approach [50] to transform multi-rate systems into single-rate systems. However, the lifting technique is primarily effective only for linear multi-rate systems, and the pseudo measurement method necessitates the introduction of an additional time judgment function, which can add complexity. In this paper, we introduce a novel approach in tackling the state estimation issue for multi-rate nonlinear SPCNs by employing the *impulsive* method. Unlike previous methods, this approach involves designing an impulse updating estimator that operates at both the state updating instant,  $p_t$ , and the sensor sampling instant,  $k_m$ . This strategy allows us to circumvent the need for

state augmentation, thereby reducing computational complexity.

#### D. Impulsive Error Dynamics

Define the state estimation error of the  $i$ -th node as

$$e_i(p_t) \triangleq x_i(p_t) - \hat{x}_i(p_t) = [e_{if}^T(p_t) \quad e_{is}^T(p_t)]^T.$$

During the time interval  $p_t \in (k_{m-1}, k_m]$  of the sensor sampling, we have

$$e_i(p_t) = A_\varepsilon e_i(p_{t-1}) + J_\varepsilon(e_i(p_{t-1})) + \sum_{j=1}^N \omega_{ij} \Gamma_\varepsilon e_j(p_{t-1}) + H_i \vartheta(p_{t-1}) \quad (15)$$

where

$$\begin{aligned} e_{if}(p_t) &\triangleq x_{if}(p_t) - \hat{x}_{if}(p_t), \\ e_{is}(p_t) &\triangleq x_{is}(p_t) - \hat{x}_{is}(p_t), \\ J_\varepsilon(e_i(p_t)) &\triangleq \begin{bmatrix} g(e_{if}(p_t)) + D e_{is}(p_t) \\ \varepsilon(h(e_{is}(p_t)) + F e_{is}(p_t)) \end{bmatrix}, \\ g(e_{if}(p_t)) &\triangleq \tilde{g}(x_{if}(p_t)) - \tilde{g}(\hat{x}_{if}(p_t)), \\ h(e_{is}(p_t)) &\triangleq \tilde{h}(x_{is}(p_t)) - \tilde{h}(\hat{x}_{is}(p_t)). \end{aligned}$$

At the specific time instant  $k_m$ , the error dynamics in our model exhibits impulsive behavior, which is a direct consequence of the estimator employing an impulsive update method. The nature of this impulsive behavior is characterized by a sudden change in the error dynamics at each  $k_m$ , which reflects the instantaneous incorporation of new sensor data into the estimation process. This impulsive update is a key feature of our approach, differentiating it from traditional continuous update methods. The detailed mathematical representation of this impulsive behavior is given as follows:

$$\begin{aligned} e_i^+(k_m) &= x_i(k_m) - \hat{x}_i^+(k_m) \\ &= e_i(k_m) - L_i(C_i e_i(k_m) - \delta_i(k_m) + M_i \vartheta(k_m)). \end{aligned} \quad (16)$$

By denoting  $e(p_t) \triangleq [e_1^T(p_t) \quad e_2^T(p_t) \quad \dots \quad e_N^T(p_t)]^T$ , the error dynamics is rewritten as the following compact form:

$$\begin{aligned} e(p_t) &= (I_N \otimes A_\varepsilon + I_N \otimes \mathcal{F}_\varepsilon) e(p_{t-1}) \\ &\quad + \varphi_\varepsilon(e(p_{t-1})) + (W \otimes \Gamma_\varepsilon) e(p_{t-1}) \\ &\quad + \mathcal{H} \nu(p_{t-1}), \quad p_t \in (k_{m-1}, k_m] \end{aligned} \quad (17)$$

and

$$e^+(k_m) = e(k_m) - \mathfrak{L} \mathcal{C} e(k_m) + \mathfrak{L} \phi(k_m) - \mathfrak{L} \mathcal{M} \nu(k_m) \quad (18)$$

where  $\otimes$  denotes the Kronecker product and

$$\begin{aligned} \mathcal{F}_\varepsilon &\triangleq \begin{bmatrix} 0 & D \\ 0 & \varepsilon F \end{bmatrix}, \quad \mathcal{M} \triangleq \text{diag}\{M_1, \dots, M_N\}, \\ \mathcal{H} &\triangleq \text{diag}\{H_1, \dots, H_N\}, \quad \nu(p_t) \triangleq \text{col}_N\{\vartheta(p_t)\}, \\ \mathfrak{L} &\triangleq \text{diag}\{L_1, \dots, L_N\}, \quad \mathcal{C} \triangleq \text{diag}\{C_1, \dots, C_N\}, \\ \phi(k_m) &\triangleq [\delta_1^T(k_m) \quad \delta_2^T(k_m) \quad \dots \quad \delta_N^T(k_m)]^T, \\ \varphi_\varepsilon(e(p_t)) &\triangleq [\varphi_{\varepsilon,1}^T(e_1(p_t)) \quad \dots \quad \varphi_{\varepsilon,N}^T(e_N(p_t))]^T, \\ \varphi_{\varepsilon,i}(e_i(p_t)) &\triangleq [g^T(e_{if}(p_t)) \quad \varepsilon h^T(e_{is}(p_t))]^T. \end{aligned}$$

Let a row-switching elementary matrix be  $R \triangleq \prod_i^N R_i$  with  $R_i \in \mathbb{R}^{n_N \times n_N}$  ( $i \in \mathcal{N}$ ). According to the properties of row-switching elementary transformation, one has  $R_i = R_i^{-1}$ . Defining  $Re(p_t) \triangleq \tilde{e}(p_t)$ , we pre-multiply (17) by the elementary matrix  $R$  to obtain

$$\tilde{e}(p_t) = \Lambda_\varepsilon \tilde{e}(p_{t-1}) + \tilde{\varphi}_\varepsilon(e(p_{t-1})) + \tilde{\mathcal{H}} \nu(p_{t-1}). \quad (19)$$

Similarly, we derive from (18) that

$$\tilde{e}^+(k_m) = \tilde{e}(k_m) - \tilde{\mathfrak{L}} \tilde{\mathcal{C}} \tilde{e}(k_m) + \tilde{\mathfrak{L}} \tilde{\phi}(k_m) - \tilde{\mathfrak{L}} \tilde{\mathcal{M}} \nu(k_m) \quad (20)$$

where

$$\begin{aligned} \Lambda_\varepsilon &\triangleq \begin{bmatrix} \Lambda^{11} & \Lambda^{12} \\ \Lambda_\varepsilon^{21} & \Lambda_\varepsilon^{22} \end{bmatrix}, \quad \tilde{\mathfrak{L}} \triangleq \begin{bmatrix} \mathfrak{L}_f & 0 \\ 0 & \mathfrak{L}_s \end{bmatrix}, \\ \mathcal{C}_f &\triangleq \text{diag}\{C_{1f}, C_{2f}, \dots, C_{Nf}\}, \\ \mathcal{C}_s &\triangleq \text{diag}\{C_{1s}, C_{2s}, \dots, C_{Ns}\}, \\ \mathfrak{L}_f &\triangleq \text{diag}\{L_{1f}, L_{2f}, \dots, L_{Nf}\}, \\ \mathfrak{L}_s &\triangleq \text{diag}\{L_{1s}, L_{2s}, \dots, L_{Ns}\}, \\ \Lambda^{11} &\triangleq I_N \otimes A_1 + W \otimes \Gamma_1, \\ \Lambda_\varepsilon^{21} &\triangleq \varepsilon(I_N \otimes A_3 + W \otimes \Gamma_3), \\ \Lambda^{12} &\triangleq I_N \otimes A_2 + I_N \otimes D + W \otimes \Gamma_2, \\ \Lambda_\varepsilon^{22} &\triangleq \varepsilon(I_N \otimes A_4 + I_N \otimes F + W \otimes \Gamma_4), \\ \tilde{\mathcal{H}} &\triangleq [\mathcal{H}_1^T \quad \mathcal{H}_2^T]^T, \quad \tilde{\mathcal{M}} \triangleq [\mathcal{M}_1^T \quad \mathcal{M}_2^T]^T, \\ \mathcal{M}_i &\triangleq \text{diag}\{M_{1i}, M_{2i}, \dots, M_{Ni}\}, \\ \mathcal{H}_i &\triangleq \text{diag}\{H_{1i}, H_{2i}, \dots, H_{Ni}\}, \quad i \in \{1, 2\}, \\ \tilde{\varphi}_\varepsilon(e(p_t)) &\triangleq [\tilde{g}^T(e_f(p_t)) \quad \varepsilon \tilde{h}^T(e_s(p_t))]^T, \\ \tilde{g}(e_f(p_t)) &\triangleq [g^T(e_{1f}(p_t)) \quad \dots \quad g^T(e_{Nf}(p_t))]^T, \\ \tilde{h}(e_s(p_t)) &\triangleq [h^T(e_{1s}(p_t)) \quad \dots \quad h^T(e_{Ns}(p_t))]^T, \\ \tilde{\phi}(k_m) &\triangleq [\tilde{\delta}_f^T(k_m) \quad \tilde{\delta}_s^T(k_m)]^T, \quad \tilde{\mathcal{C}} \triangleq \begin{bmatrix} \mathcal{C}_f & 0 \\ 0 & \mathcal{C}_s \end{bmatrix}, \\ \tilde{\delta}_f(k_m) &\triangleq \begin{bmatrix} y_{1f}(k_m) - \tilde{y}_{1f}(k_m) \\ \vdots \\ y_{Nf}(k_m) - \tilde{y}_{Nf}(k_m) \end{bmatrix}^T, \\ \tilde{\delta}_s(k_m) &\triangleq \begin{bmatrix} y_{1s}(k_m) - \tilde{y}_{1s}(k_m) \\ \vdots \\ y_{Ns}(k_m) - \tilde{y}_{Ns}(k_m) \end{bmatrix}^T. \end{aligned}$$

**Lemma 1:** [31] For a positive scalar  $\varepsilon$ , and  $\Omega_1$  and  $\Omega_2$  be symmetric matrices with compatible dimensions. Then, the following inequality

$$\Omega_1 + \varepsilon \Omega_2 < 0, \quad \varepsilon \in (0, \varepsilon] \quad (21)$$

holds if and only if  $\Omega_1 \leq 0$  and  $\Omega_1 + \varepsilon \Omega_2 < 0$ .

**Definition 1:** The estimation error dynamics of SPCNs is said to be ultimately exponentially bounded if there exist scalars  $0 < \bar{a}_1 < 1$ ,  $\bar{a}_2 > 0$  and  $\bar{a}_3 > 0$  such that the following inequality holds:

$$\|\tilde{e}(p_t)\|^2 \leq \bar{a}_1^{p_t} \bar{a}_2 + \bar{a}_3 \quad (22)$$

where  $\bar{a}_3$  is an asymptotic upper bound of the error  $\|\tilde{e}(p_t)\|^2$ .

### III. MAIN RESULTS

#### A. Boundedness Analysis

In the following theorem, a sufficient condition is given to analyze the ultimate boundedness of the error dynamics.

*Theorem 1:* Let the scalars  $\beta_1 > 1$ ,  $0 < \beta_2 < 1$ ,  $\varepsilon > 0$ , the positive integers  $B_i$  ( $i \in \mathcal{N}$ ) and the estimator gains be given. If there exist positive scalars  $\epsilon_1, \epsilon_2, \tau_1, \tau_2, \tau_3$  and positive definite matrix  $P_\varepsilon$  such that the following inequalities hold:

$$\begin{bmatrix} \Pi_{11} & \Pi_{12} \\ * & -P_\varepsilon^{-1} \end{bmatrix} < 0 \quad (23)$$

$$\begin{bmatrix} \Omega_{11} & \Omega_{12} \\ * & -P_\varepsilon^{-1} \end{bmatrix} < 0 \quad (24)$$

$$0 < \beta_1^b \beta_2 < 1 \quad (25)$$

where

$$\Pi_{11} \triangleq \begin{bmatrix} -\beta_1 P_\varepsilon - \mathfrak{J}_{11} & \mathfrak{J}_{12} & \mathfrak{J}_{13} & 0 \\ * & -\epsilon_1 I_{n_f N} & 0 & 0 \\ * & * & -\epsilon_2 I_{n_s N} & 0 \\ * & * & * & -\tau_1 I_{\zeta N} \end{bmatrix},$$

$$\Pi_{12} \triangleq [\Lambda_\varepsilon \quad Z_f \quad \varepsilon Z_s \quad \tilde{\mathcal{H}}]^T,$$

$$\Omega_{11} \triangleq \begin{bmatrix} -\beta_2 P_\varepsilon & 0 & 0 \\ 0 & -\tau_2 I_{vN} & 0 \\ 0 & 0 & -\tau_3 I_{\zeta N} \end{bmatrix},$$

$$\Omega_{12} \triangleq [I_{nN} - \tilde{\mathcal{L}}\tilde{\mathcal{C}} \quad \tilde{\mathcal{L}} \quad -\tilde{\mathcal{L}}\tilde{\mathcal{M}}]^T,$$

$$\mathfrak{J}_{11} \triangleq \epsilon_1 Z_f \psi_1^T \psi_2 Z_f^T + \epsilon_2 Z_s \chi_1^T \chi_2 Z_s^T,$$

$$\mathfrak{J}_{12} \triangleq \epsilon_1 Z_f \frac{\psi_1^T + \psi_2^T}{2}, \quad \mathfrak{J}_{13} \triangleq \epsilon_2 Z_s \frac{\chi_1^T + \chi_2^T}{2},$$

$$\psi_i \triangleq I_N \otimes \tilde{\psi}_i, \quad \chi_i \triangleq I_N \otimes \tilde{\chi}_i, \quad i \in \{1, 2\},$$

$$Z_f \triangleq \begin{bmatrix} I_{n_f N} \\ 0_{n_s N \times n_f N} \end{bmatrix}, \quad Z_s \triangleq \begin{bmatrix} 0_{n_f N \times n_s N} \\ I_{n_s N} \end{bmatrix},$$

then the estimation error dynamics is ultimately exponentially bounded.

*Proof:* Choose the Lyapunov-like functional candidate as

$$V(p_t) = \tilde{e}^T(p_t) P_\varepsilon \tilde{e}(p_t). \quad (26)$$

Let the difference of  $V(p_t)$  at the time interval  $p_t \in (k_{m-1}, k_m]$  be

$$\Delta V(p_t) \triangleq V(p_t) - \beta_1 V(p_{t-1}).$$

Combining (19) and (26), one has

$$\begin{aligned} \Delta V(p_t) &= \tilde{e}^T(p_{t-1}) \Lambda_\varepsilon^T P_\varepsilon \Lambda_\varepsilon \tilde{e}(p_{t-1}) + \tilde{\varphi}_\varepsilon^T(e(p_{t-1})) P_\varepsilon \\ &\quad \times \tilde{\varphi}_\varepsilon(e(p_{t-1})) + 2\tilde{e}^T(p_{t-1}) \Lambda_\varepsilon^T P_\varepsilon \tilde{\varphi}_\varepsilon(e(p_{t-1})) \\ &\quad + \nu^T(p_{t-1}) \tilde{\mathcal{H}}^T P_\varepsilon \tilde{\mathcal{H}} \nu(p_{t-1}) - \beta_1 \tilde{e}^T(p_{t-1}) P_\varepsilon \\ &\quad \times \tilde{e}(p_{t-1}) + 2\tilde{e}^T(p_{t-1}) \Lambda_\varepsilon^T P_\varepsilon \tilde{\mathcal{H}} \nu(p_{t-1}) \\ &\quad + 2\tilde{\varphi}_\varepsilon^T(e(p_{t-1})) P_\varepsilon \tilde{\mathcal{H}} \nu(p_{t-1}). \end{aligned} \quad (27)$$

Letting  $\tilde{\varphi}_\varepsilon(e(p_t)) \triangleq Z_f \check{g}(e_f(p_t)) + \varepsilon Z_s \check{h}(e_s(p_t))$ , we rewrite (27) as follows:

$$\Delta V(p_t) = \tilde{e}^T(p_{t-1}) \Lambda_\varepsilon^T P_\varepsilon \Lambda_\varepsilon \tilde{e}(p_{t-1}) + \check{g}^T(e_f(p_{t-1})) Z_f^T$$

$$\begin{aligned} &\times P_\varepsilon Z_f \check{g}(e_f(p_{t-1})) + \varepsilon^2 \check{h}^T(e_s(p_{t-1})) Z_s^T P_\varepsilon \\ &\times Z_s \check{h}(e_s(p_{t-1})) + 2\check{g}^T(e_f(p_{t-1})) Z_f^T P_\varepsilon Z_s \\ &\times \check{h}(e_s(p_{t-1})) + 2\tilde{e}^T(p_{t-1}) \Lambda_\varepsilon^T P_\varepsilon Z_f \check{g}(e_f(p_{t-1})) \\ &+ 2\tilde{e}^T(p_{t-1}) \Lambda_\varepsilon^T P_\varepsilon Z_s \check{h}(e_s(p_{t-1})) \\ &+ 2\varepsilon \check{h}^T(e_s(p_{t-1})) Z_s^T P_\varepsilon \tilde{\mathcal{H}} \nu(p_{t-1}) + \nu^T(p_{t-1}) \\ &\times \tilde{\mathcal{H}}^T P_\varepsilon \tilde{\mathcal{H}} \nu(p_{t-1}) + 2\tilde{e}^T(p_{t-1}) \Lambda_\varepsilon^T P_\varepsilon \tilde{\mathcal{H}} \\ &\times \nu(p_{t-1}) + 2\check{g}^T(e_f(p_{t-1})) Z_f^T P_\varepsilon \tilde{\mathcal{H}} \nu(p_{t-1}) \\ &- \beta_1 \tilde{e}^T(p_{t-1}) P_\varepsilon \tilde{e}(p_{t-1}). \end{aligned} \quad (28)$$

It follows from the nonlinearity conditions in (2) and (3) that, for any scalars  $\epsilon_1 > 0$  and  $\epsilon_2 > 0$ , the following are true:

$$\begin{aligned} \epsilon_1 (\check{g}(e_f(p_t)) - \psi_1 e_f(p_t))^T (\check{g}(e_f(p_t)) - \psi_2 e_f(p_t)) &\leq 0, \\ \epsilon_2 (\check{h}(e_s(p_t)) - \chi_1 e_s(p_t))^T (\check{h}(e_s(p_t)) - \chi_2 e_s(p_t)) &\leq 0. \end{aligned} \quad (29)$$

Substituting  $e_f(p_t) = Z_f^T \tilde{e}(p_t)$  and  $e_s(p_t) = Z_s^T \tilde{e}(p_t)$  into (29), we have

$$\begin{bmatrix} \tilde{e}(p_t) \\ \check{g}(e_f(p_t)) \\ \check{h}(e_s(p_t)) \end{bmatrix}^T \begin{bmatrix} \mathfrak{J}_{11} & -\mathfrak{J}_{12} & -\mathfrak{J}_{13} \\ * & \epsilon_1 I_{n_f N} & 0 \\ * & * & \epsilon_2 I_{n_s N} \end{bmatrix} \begin{bmatrix} \tilde{e}(p_t) \\ \check{g}(e_f(p_t)) \\ \check{h}(e_s(p_t)) \end{bmatrix} \leq 0. \quad (30)$$

Define an augmented vector as

$$\xi(p_t) \triangleq [\tilde{e}^T(p_t) \quad \check{g}^T(e_f(p_t)) \quad \check{h}^T(e_s(p_t)) \quad \nu^T(p_t)]^T.$$

Combining the difference function (28) and nonlinear constraint (30), we obtain

$$\Delta V(p_t) \leq \xi^T(p_{t-1}) \tilde{\Pi} \xi(p_{t-1}) + \tau_1 \nu^T(p_{t-1}) \nu(p_{t-1}) \quad (31)$$

where

$$\tilde{\Pi} \triangleq \begin{bmatrix} \tilde{\Pi}_{11} & \tilde{\Pi}_{12} & \tilde{\Pi}_{13} & \tilde{\Pi}_{14} \\ * & \tilde{\Pi}_{22} & \tilde{\Pi}_{23} & \tilde{\Pi}_{24} \\ * & * & \tilde{\Pi}_{33} & \tilde{\Pi}_{34} \\ * & * & * & \tilde{\Pi}_{44} \end{bmatrix},$$

$$\tilde{\Pi}_{11} \triangleq \Lambda_\varepsilon^T P_\varepsilon \Lambda_\varepsilon - \beta_1 P_\varepsilon - \mathfrak{J}_{11}, \quad \tilde{\Pi}_{12} \triangleq \Lambda_\varepsilon^T P_\varepsilon Z_f + \mathfrak{J}_{12},$$

$$\tilde{\Pi}_{13} \triangleq \varepsilon \Lambda_\varepsilon^T P_\varepsilon Z_s + \mathfrak{J}_{13}, \quad \tilde{\Pi}_{14} \triangleq \Lambda_\varepsilon^T P_\varepsilon \tilde{\mathcal{H}},$$

$$\tilde{\Pi}_{22} \triangleq Z_f^T P_\varepsilon Z_f - \epsilon_1 I_{n_f N}, \quad \tilde{\Pi}_{23} \triangleq \varepsilon Z_f^T P_\varepsilon Z_s,$$

$$\tilde{\Pi}_{24} \triangleq Z_f^T P_\varepsilon \tilde{\mathcal{H}}, \quad \tilde{\Pi}_{33} \triangleq \varepsilon^2 Z_s^T P_\varepsilon Z_s - \epsilon_2 I_{n_s N},$$

$$\tilde{\Pi}_{34} \triangleq \varepsilon Z_s^T P_\varepsilon \tilde{\mathcal{H}}, \quad \tilde{\Pi}_{44} \triangleq \tilde{\mathcal{H}}^T P_\varepsilon \tilde{\mathcal{H}} - \tau_1 I_{\zeta N}.$$

Applying Schur Complement Lemma to (23) in Theorem 1, we have  $\tilde{\Pi} < 0$ , which implies

$$\Delta V(p_t) < \tau_1 \nu^T(p_{t-1}) \nu(p_{t-1}). \quad (32)$$

For the sake of simplicity, we denote  $\tilde{\pi}_1 \triangleq \tau_1 N \vartheta_0^2$ . Subsequently, the inequality (32) is further expressed as

$$V(p_t) < \beta_1 V(p_{t-1}) + \tilde{\pi}_1, \quad p_t \in (k_{m-1}, k_m]. \quad (33)$$

Let us continue to analyze the difference function at the time instant  $p_t = k_m$ . Denoting

$$\Delta V^+(k_m) \triangleq V^+(k_m) - \beta_2 V(k_m),$$

$$\hat{\xi}(k_m) \triangleq [\tilde{e}^T(k_m) \quad \tilde{\phi}^T(k_m) \quad \nu^T(k_m)]^T,$$

one obtains

$$\Delta V^+(k_m) = \hat{\xi}^T(k_m) \tilde{\Omega} \hat{\xi}(k_m) + \tau_2 \tilde{\phi}^T(k_m) \tilde{\phi}(k_m) + \tau_3 \nu^T(k_m) \nu(k_m) \quad (34)$$

where

$$\tilde{\Omega} \triangleq \begin{bmatrix} \tilde{\Omega}_{11} & \tilde{\Omega}_{12} & \tilde{\Omega}_{13} \\ * & \tilde{\Omega}_{22} & \tilde{\Omega}_{23} \\ * & * & \tilde{\Omega}_{33} \end{bmatrix},$$

$$\tilde{\Omega}_{11} \triangleq (I_{nN} - \tilde{\mathcal{L}}\tilde{\mathcal{C}})^T P_\varepsilon (I_{nN} - \tilde{\mathcal{L}}\tilde{\mathcal{C}}) - \beta_2 P_\varepsilon,$$

$$\tilde{\Omega}_{13} \triangleq -(I_{nN} - \tilde{\mathcal{L}}\tilde{\mathcal{C}})^T P_\varepsilon \tilde{\mathcal{L}}\tilde{\mathcal{M}}, \quad \tilde{\Omega}_{23} \triangleq -\tilde{\mathcal{L}}^T P_\varepsilon \tilde{\mathcal{L}}\tilde{\mathcal{M}},$$

$$\tilde{\Omega}_{22} \triangleq \tilde{\mathcal{L}}^T P_\varepsilon \tilde{\mathcal{L}} - \tau_2 I_{vN}, \quad \tilde{\Omega}_{12} \triangleq (I_{nN} - \tilde{\mathcal{L}}\tilde{\mathcal{C}})^T P_\varepsilon \tilde{\mathcal{L}},$$

$$\tilde{\Omega}_{33} \triangleq \tilde{\mathcal{M}}^T \tilde{\mathcal{L}}^T P_\varepsilon \tilde{\mathcal{L}}\tilde{\mathcal{M}} - \tau_3 I_{\zeta N}.$$

We derive  $\tilde{\Omega} < 0$  by using the Schur Complement Lemma to (24) and, furthermore, we obtain

$$V^+(k_m) < \beta_2 V(k_m) + \tau_2 \tilde{\phi}^T(k_m) \tilde{\phi}(k_m) + \tau_3 \nu^T(k_m) \nu(k_m). \quad (35)$$

From the quantization error (10), it follows that

$$\|\tilde{\phi}(k_m)\|^2 \leq \sum_{i=1}^N v \sigma_i^2 / \hat{q}_i^2 \quad (36)$$

and we can further conclude from (35) and (36) that

$$V^+(k_m) < \beta_2 V(k_m) + \tilde{\pi}_2 \quad (37)$$

with  $\tilde{\pi}_2 \triangleq \tau_2 \sum_{i=1}^N v \sigma_i^2 / [\sqrt{2B_i}]^2 + \tau_3 N \vartheta_0^2$ .

In view of inequalities (33) and (37), the energy function is derived through a series of iterations. The following relations are established over the interval  $(k_0, k_2]$ :

$$V(p_t) < \beta_1^t V(p_0) + \sum_{j=0}^{t-1} \beta_1^j \tilde{\pi}_1, \quad p_t \in (k_0, k_1],$$

$$V^+(k_1) < \beta_1^b \beta_2 V(p_0) + \beta_2 \sum_{j=0}^{b-1} \beta_1^j \tilde{\pi}_1 + \tilde{\pi}_2,$$

$$V(p_t) < \beta_1^b \beta_2 V(p_0) + \sum_{j=0}^{t-b-1} \beta_1^j \tilde{\pi}_1 + \beta_1^{t-b} \tilde{\pi}_2$$

$$+ \beta_2 \sum_{j=t-b}^{t-1} \beta_1^j \tilde{\pi}_1, \quad p_t \in (k_1, k_2],$$

$$V^+(k_2) < \beta_1^{2b} \beta_2^2 V(p_0) + \beta_2 \sum_{j=0}^{b-1} \beta_1^j \tilde{\pi}_1$$

$$+ \beta_2^2 \sum_{j=b}^{2b-1} \beta_1^j \tilde{\pi}_1 + \beta_1^b \beta_2 \tilde{\pi}_2 + \tilde{\pi}_2.$$

Similarly, utilizing mathematical induction (a method of logical deduction), we conclude the relation in an arbitrary interval  $(k_{m-1}, k_m]$  as

$$V(p_t) < \beta_1^t \beta_2^{m-1} V(p_0) + \sum_{j=0}^{t-k_{m-1}-1} \beta_1^j \tilde{\pi}_1$$

$$+ \beta_2 \sum_{j=t-k_{m-1}}^{t-k_{m-2}-1} \beta_1^j \tilde{\pi}_1 + \dots + \beta_2^{m-1} \sum_{j=t-k_1}^{t-1} \beta_1^j \tilde{\pi}_1$$

$$+ \sum_{\tau=2}^m \beta_2^{m-\tau} \beta_1^{t-k_{\tau-1}} \tilde{\pi}_2, \quad p_t \in (k_{m-1}, k_m]. \quad (38)$$

Based on the nature of the coefficients  $\beta_1$  and  $\beta_2$ , we perform a further operation on (38) as follows:

$$V(p_t) < \beta_1^t \beta_2^{m-1} V(p_0) + \sum_{j=0}^{t-(m-1)b-1} \beta_1^j \tilde{\pi}_1$$

$$+ \beta_2 \sum_{j=t-(m-1)b}^{t-(m-2)b-1} \beta_1^j \tilde{\pi}_1 + \dots + \beta_2^{m-1} \sum_{j=t-b}^{mb-1} \beta_1^j \tilde{\pi}_1$$

$$+ \left( \beta_2^{m-2} \beta_1^{t-b} + \beta_2^{m-3} \beta_1^{t-2b} + \dots + \beta_1^{t-(m-1)b} \right) \tilde{\pi}_2$$

$$= \beta_1 (\beta_1^b \beta_2)^{m-1} V(p_0) + \sum_{\tau=0}^{m-1} (\beta_1^b \beta_2)^\tau \sum_{j=0}^{b-1} \beta_1^j \tilde{\pi}_1$$

$$+ \beta_1 \tilde{\pi}_2 \sum_{\tau=0}^{m-2} (\beta_1^b \beta_2)^\tau + \beta_1^b \tilde{\pi}_2 - \beta_1 \tilde{\pi}_2, \quad (39)$$

which further indicates

$$V(p_t) < \beta_1 (\beta_1^b \beta_2)^{m-1} V(p_0) + \left( \frac{1}{1 - \beta_1^b \beta_2} - 1 \right) \beta_1 \tilde{\pi}_2$$

$$+ \beta_1^b \tilde{\pi}_2 + \frac{1}{1 - \beta_1^b \beta_2} \sum_{j=0}^{b-1} \beta_1^j \tilde{\pi}_1, \quad m \rightarrow \infty. \quad (40)$$

According to the expression of Lyapunov-like functional candidate in (26), one can conclude that

$$\|\tilde{e}(p_t)\|^2 < \frac{\beta_1 (\beta_1^b \beta_2)^{m-1}}{\lambda_{\min}(P_\varepsilon)} V(p_0) + \tilde{\delta} \quad (41)$$

where

$$\tilde{\delta} \triangleq \frac{\left( \frac{1}{1 - \beta_1^b \beta_2} - 1 \right) \beta_1 \tilde{\pi}_2 + \beta_1^b \tilde{\pi}_2 + \frac{1}{1 - \beta_1^b \beta_2} \sum_{j=0}^{b-1} \beta_1^j \tilde{\pi}_1}{\lambda_{\min}(P_\varepsilon)}.$$

Reviewing the condition (25), when  $p_t$  goes to infinity (i.e.  $k_m \rightarrow \infty, m \rightarrow \infty$ ), we have

$$\|\tilde{e}(p_t)\|^2 < \tilde{\delta}, \quad (42)$$

which ends the proof.  $\blacksquare$

*Remark 4:* As indicated by the parameter  $\tilde{\pi}_2$  of the estimation error bound, we can infer that the error bound  $\tilde{\delta}$  is influenced by various factors, including bounded noise, coding-decoding parameters  $\sigma_i$ , bit rate  $B_i$ , sampling parameter  $b$ , and convergence coefficients  $\beta_1$  and  $\beta_2$ . When all system parameters,  $\sigma_i$  and  $b$  are fixed, the error bound is directly determined by the bit rate  $B_i$  of each node. Specifically, an increasing  $B_i$  results a higher maximum quantization level  $\hat{q}_i$ , leading to reduced decoding errors and, consequently, a decreasing error bound. This relation emphasizes the critical role of bit rate in reducing estimation errors in digital communication networks.

## B. Impulsive Estimator Gain Design

Based on Theorem 1 and Lemma 1, the following theorem is presented to highlight the basic procedure in obtaining the desired estimator gains.

**Theorem 2:** Let scalars  $\beta_1 > 1$ ,  $0 < \beta_2 < 1$ ,  $\varepsilon > 0$  and positive integers  $B_i$  ( $i \in \mathcal{N}$ ) be given. The error dynamics is ultimately bounded if there exist positive scalars  $\epsilon_1, \epsilon_2, \tau_1, \tau_2, \tau_3$ , matrices  $\check{P}, \check{P}, \mathcal{K}$ , and non-singular matrix  $Q$  such that (25) and the following inequalities hold:

$$\begin{bmatrix} \check{\Pi}_{11} & \check{\Pi}_{12} \\ * & \check{\Omega} \end{bmatrix} \leq 0 \quad (43)$$

$$\begin{bmatrix} \hat{\Pi}_{11} & \hat{\Pi}_{12} \\ * & \hat{\Omega} \end{bmatrix} < 0 \quad (44)$$

$$\begin{bmatrix} \check{\Omega}_{11} & \check{\Omega}_{12} \\ * & \check{\Omega} \end{bmatrix} \leq 0 \quad (45)$$

$$\begin{bmatrix} \hat{\Omega}_{11} & \hat{\Omega}_{12} \\ * & \hat{\Omega} \end{bmatrix} < 0 \quad (46)$$

$$\check{P} \geq 0, \check{P} + \varepsilon \hat{P} > 0 \quad (47)$$

where

$$\check{\Pi}_{11} \triangleq \begin{bmatrix} -\beta_1 \check{P} - \check{\mathfrak{J}}_{11} & \check{\mathfrak{J}}_{12} & \check{\mathfrak{J}}_{13} & 0 \\ * & -\epsilon_1 I_{n_f N} & 0 & 0 \\ * & * & -\epsilon_2 I_{n_s N} & 0 \\ * & * & * & -\tau_1 I_{\zeta N} \end{bmatrix},$$

$$\hat{\Pi}_{11} \triangleq \begin{bmatrix} -\beta_1(\check{P} + \varepsilon \hat{P}) - \check{\mathfrak{J}}_{11} & \check{\mathfrak{J}}_{12} & \check{\mathfrak{J}}_{13} & 0 \\ * & -\epsilon_1 I_{n_f N} & 0 & 0 \\ * & * & -\epsilon_2 I_{n_s N} & 0 \\ * & * & * & -\tau_1 I_{\zeta N} \end{bmatrix},$$

$$\check{\Omega}_{11} \triangleq \begin{bmatrix} -\beta_2 \check{P} & 0 & 0 \\ 0 & -\tau_2 I_{vN} & 0 \\ 0 & 0 & -\tau_3 I_{\zeta N} \end{bmatrix},$$

$$\hat{\Omega}_{11} \triangleq \begin{bmatrix} -\beta_2(\check{P} + \varepsilon \hat{P}) & 0 & 0 \\ 0 & -\tau_2 I_{vN} & 0 \\ 0 & 0 & -\tau_3 I_{\zeta N} \end{bmatrix},$$

$$\check{\Pi}_{12} \triangleq [\Upsilon_0^T \quad QZ_f \quad 0 \quad Q\tilde{\mathcal{H}}]^T,$$

$$\hat{\Pi}_{12} \triangleq [\Upsilon_0^T + \varepsilon \Upsilon_1^T \quad QZ_f \quad \varepsilon QZ_s \quad Q\tilde{\mathcal{H}}]^T,$$

$$\check{\Omega}_{12} \triangleq [Q - \mathcal{K}\tilde{\mathcal{C}} \quad \mathcal{K} \quad -\mathcal{K}\tilde{\mathcal{M}}]^T, \quad Q \triangleq \text{diag}\{Q_f, Q_s\},$$

$$\Upsilon_0 \triangleq \begin{bmatrix} (\Lambda^{11})^T Q_f^T & 0 \\ (\Lambda^{12})^T & 0 \end{bmatrix}, \quad \mathcal{K} \triangleq \text{diag}\{\mathcal{K}_f, \mathcal{K}_s\},$$

$$\Upsilon_1 \triangleq \begin{bmatrix} 0 & (I_N \otimes A_3 + W \otimes \Gamma_3)^T \\ 0 & (I_N \otimes A_4 + I_N \otimes F + W \otimes \Gamma_4)^T Q_s^T \end{bmatrix},$$

$$\check{\Omega} \triangleq \check{P} - Q - Q^T, \quad \hat{\Omega} \triangleq (\check{P} + \varepsilon \hat{P}) - Q - Q^T,$$

$$Q_f \triangleq \text{diag}\{Q_{1f}, \dots, Q_{Nf}\}, \quad Q_s \triangleq \text{diag}\{Q_{1s}, \dots, Q_{Ns}\},$$

$$\mathcal{K}_f \triangleq \text{diag}\{\mathcal{K}_{1f}, \dots, \mathcal{K}_{Nf}\}, \quad \mathcal{K}_s \triangleq \text{diag}\{\mathcal{K}_{1s}, \dots, \mathcal{K}_{Ns}\}.$$

Furthermore, the gains of the impulsive estimator are given by  $L_{if} = Q_{if}^{-1} \mathcal{K}_{if}$ , and  $L_{is} = Q_{is}^{-1} \mathcal{K}_{is}$ .

*Proof:* From (43), (44) and Lemma 1, one has

$$\begin{bmatrix} \check{\Xi}_{11} & \check{\Xi}_{12} \\ * & \check{\Omega} + \varepsilon \hat{P} \end{bmatrix} < 0 \quad (48)$$

where

$$\check{\Xi}_{11} \triangleq \begin{bmatrix} -\beta_1(\check{P} + \varepsilon \hat{P}) - \check{\mathfrak{J}}_{11} & \check{\mathfrak{J}}_{12} & \check{\mathfrak{J}}_{13} & 0 \\ * & -\epsilon_1 I_{n_f N} & 0 & 0 \\ * & * & -\epsilon_2 I_{n_s N} & 0 \\ * & * & * & -\tau_1 I_{\zeta N} \end{bmatrix},$$

$$\check{\Xi}_{12} \triangleq [\Upsilon_0^T + \varepsilon \Upsilon_1^T \quad QZ_f \quad \varepsilon QZ_s \quad Q\tilde{\mathcal{H}}]^T.$$

Define  $P_\varepsilon \triangleq \check{P} + \varepsilon \hat{P}$ ,  $\varepsilon \in (0, \varepsilon]$ . It follows from (47) and Lemma 1 that

$$\check{P} + \varepsilon \hat{P} > 0. \quad (49)$$

Based on the relation  $(P_\varepsilon - Q)P_\varepsilon^{-1}(P_\varepsilon - Q)^T \geq 0$ , we have

$$P_\varepsilon - Q - Q^T \geq -QP_\varepsilon^{-1}Q^T. \quad (50)$$

Let  $\mathbb{I}$  denote the identify matrix with proper dimension, and  $\mathcal{K} \triangleq Q\tilde{\mathcal{C}}$ . By applying (50) into (48), and pre-multiplying it with  $\mathbb{Q} \triangleq \text{diag}\{\mathbb{I}, Q\}$  and post-multiplying it with  $\mathbb{Q}^T$ , we can conclude that the inequality (48) holds under the condition (23). The similar method is employed to prove the conditions (45) and (46). The proof is now complete. ■

## C. Co-design of Bit Rate Allocation Strategy and Estimator

For each sensor node  $i$  ( $i \in \mathcal{N}$ ), the impulsive estimator is designed by allocating specific bit rates, as detailed in Theorem 2. As highlighted in equation (41), the selected bit rate  $B_i$  for each sensor significantly affects the upper bound of the estimation error, thereby influencing the overall performance of the state estimation. The primary goal of this section is to improve the overall estimation performance, which is achieved by *jointly* optimizing the bit rate allocation for each sensor and the gains of the estimator. The optimization process is approached as a minimization problem, aiming to find the optimal combination of bit rates and estimator gains that minimizes the error upper bound, thereby enhancing the accuracy and efficiency of the state estimation process in the network.

*Corollary 1:* According to Theorem 2, when the assigned bit rate  $B_i$  ( $i \in \mathcal{N}$ ) is the variable to be designed, the optimization problem for the error upper bound is reformulated as the following minimization task:

$$\begin{aligned} \min & \frac{\mathcal{Z}_1 \left( \tau_2 \sum_{i=1}^N v \sigma_i^2 / [\sqrt{2^{B_i}}]^2 + \tau_3 N \vartheta_0^2 \right) + \mathcal{Z}_2}{\lambda_{\min}(P_\varepsilon)} \\ \text{s.t.} & \text{ (5), (25), (43) - (47), } 0 \leq B_i \leq B \end{aligned} \quad (51)$$

where

$$\mathcal{Z}_1 \triangleq (1/(1 - \beta_1^b \beta_2) - 1) \beta_1 + \beta_1^b,$$

$$\mathcal{Z}_2 \triangleq 1/(1 - \beta_1^b \beta_2) \sum_{j=0}^{b-1} \beta_1^j \tilde{\pi}_1.$$

Within this framework, the impulsive estimator gains are designed as  $L_{if} = Q_{if}^{-1} \mathcal{K}_{if}$  and  $L_{is} = Q_{is}^{-1} \mathcal{K}_{is}$ .

*Proof:* The proof is similar to that of Theorem 2, and is therefore omitted here for space saving. ■

The minimization problem formulated in (51) is characterized as non-convex, which presents a significant challenge for traditional solution methods. To address this complexity, we propose a novel co-design approach that combines the particle swarm optimization (PSO) algorithm with the linear matrix inequality (LMI) technique, allowing for a more effective and reliable solution to the optimization of bit rate allocation and estimator gains.

Considering that the above minimization problem contains the constraint term  $0 \leq B_i \leq B$ , we transform (51) into the following form by introducing a penalty function:

$$\min \frac{\mathcal{Z}_1 \left( \tau_2 \sum_{i=1}^N v\sigma_i^2 / [\sqrt{2B_i}]^2 + \tau_3 N \vartheta_0^2 \right) + \mathcal{Z}_2}{\lambda_{\min}(P_\varepsilon)} + \eta \mathcal{J}(\bar{B})$$

s.t. (25), (43) – (47) (52)

where  $\mathcal{J}(\bar{B}) \triangleq \max \left\{ 0, \sum_{i=1}^N B_i - B \right\}$  is the exterior penalty function with  $\bar{B} \triangleq [B_1, B_2, \dots, B_N]$ , and  $\eta$  is a constant called penalty coefficient. The fitness function of PSO algorithm is the error upper bound, which is defined as

$$\mathbf{F}(\bar{B}) \triangleq \frac{\mathcal{Z}_1 \left( \tau_2 \sum_{i=1}^N v\sigma_i^2 / [\sqrt{2B_i}]^2 + \tau_3 N \vartheta_0^2 \right) + \mathcal{Z}_2}{\lambda_{\min}(P_\varepsilon)} + \eta \mathcal{J}(\bar{B}). \quad (53)$$

Derived from the aforementioned objective function, Algorithm 1 presents a comprehensive framework for estimator design, seamlessly combining the PSO algorithm with the LMI technique. This algorithm is devised to address the minimization problem associated with the objective function, accounting for constraints and nonlinearity. In Algorithm 1,  $\mathbf{X}_i \triangleq [\mathbf{X}_{i,1}, \mathbf{X}_{i,2}, \dots, \mathbf{X}_{i,N}]$  and  $\mathbf{V}_i \triangleq [\mathbf{V}_{i,1}, \mathbf{V}_{i,2}, \dots, \mathbf{V}_{i,N}]$  denote the position and velocity of the  $i$ -th particle, respectively;  $N$  is the number of particles in the search space, and the maximum number of iterations is represented by  $\mathbf{I}$ . The update of particle velocity and position obeys the following equations:

$$\mathbf{V}_i(\kappa + 1) = \mathbf{w}\mathbf{V}_i(\kappa) + \mathbf{c}_1 \xi_1 (\mathbf{P}_i(\kappa) - \mathbf{X}_i(\kappa)) + \mathbf{c}_2 \xi_2 (\mathbf{P}_g(\kappa) - \mathbf{X}_i(\kappa)), \quad (54)$$

$$\mathbf{X}_i(\kappa + 1) = \mathbf{X}_i(\kappa) + \mathbf{V}_i(\kappa) \quad (55)$$

where  $\kappa \in [1, 2, \dots, \mathbf{I}]$  indicates the iteration number;  $\mathbf{w}$  stands for the inertia weight; the acceleration constants  $\mathbf{c}_1$  and  $\mathbf{c}_2$  denote the self-learning factor and the group learning factor, respectively;  $\xi_1$  and  $\xi_2$  are two stochastic integers distributed in the interval  $[1, 2]$ .  $\mathbf{P}_i$  denotes the position of particle  $i$  after updating.  $\mathbf{P}_g$  represents the particle position corresponding to the historical minimum fitness function of the particle swarm. In order to avoid the particle's search position from surpassing the limited interval and prevent an unproductive search, well-defined boundaries are established for both position and velocity. These boundaries, denoted as  $\mathbf{X}_T$  (upper bound),  $\mathbf{X}_L$  (lower bound) for position, as well as  $\mathbf{V}_T$  (upper bound),  $\mathbf{V}_L$  (lower bound) for velocity, play a crucial role in constraining the particle's movement within a controlled and purposeful range.

By applying this algorithm, an optimal bit rate allocation strategy can be obtained, which can further advance a comprehensive analysis of different bit rates' effects on the estimation performance of multi-rate SPCNs.

---

**Algorithm 1:** Co-design assisted by PSO Algorithm

---

- Step 1.** *Parameter initialization:* Initialize parameters  $N$ ,  $\mathbf{I}$ ,  $\mathbf{w}$ ,  $\mathbf{c}_1$ ,  $\mathbf{c}_2$ , position  $\mathbf{X}_i$ , and velocity  $\mathbf{V}_i$  of each particle ( $i \in \{1, 2, \dots, N\}$ ).
- Step 2.** *Fitness update:* For each particle, update the fitness function  $\mathbf{F}(\mathbf{X}_i)$  if the feasible solutions for LMIs (43)-(47) exist; otherwise, set  $\mathbf{F}(\mathbf{X}_i) = \infty$ .
- Step 3.** Select the particle with the minimum fitness function in the population and record its position  $\mathbf{P}_i$ .
- Step 4.** *Particle swarm update:* Update the velocity and position of the particle swarm according to formulas (54) and (55), and correct it based on the boundary constraints.
- Step 5.** *Fitness function and position update:* Solve LMIs (43)-(47) using the updated positions in Step 4, and obtain the updated fitness function  $\mathbf{F}(\mathbf{X}_i)$  if there is a feasible solution, otherwise, set  $\mathbf{F}(\mathbf{X}_i)$  as infinity. Record updated particle's position  $\mathbf{P}_i$ .
- Step 6.** Search for particle swarm history minimum fitness and its corresponding position  $\mathbf{P}_g$ .
- Step 7.** *Bit rate allocation protocol design:* Repeat Steps 4 to 6 in a loop until the iteration is terminated. Get the particle with the minimum fitness, whose corresponding position is the optimal bit-rate allocation scheme.
- Step 8.** *Design the impulsive estimator:* The estimator gains  $L_{if}$  and  $L_{is}$  are obtained by solving LMIs (43)-(47) under optimal bit rate allocation protocol (i.e. position  $\mathbf{P}_g$ ).
- 

*Remark 5:* This paper introduces several novel contributions to the field of state estimation for SPCNs, particularly distinguishing itself from existing research in the following key ways. 1) For the first time, this study addresses discrete-time multi-rate SPCNs within the context of digital communication networks, placing a special emphasis on the constrained bit rate of wireless networks. 2) We pioneer the use of the impulsive method for designing state estimators in multi-rate systems. This method allows us to derive upper bounds on error dynamics within the framework of impulse analysis. Theorem 2 provides insights into the derivation of estimator gains, which are determined based on a specific allocation of bit rates to each sensor. 3) By employing the PSO algorithm, the paper focuses on minimizing an objective function that encompasses the error upper bound. 4) A co-design approach is proposed that involves both the optimization of estimator gains and the development of a bit-rate allocation protocol. This strategy is aimed at enhancing the overall estimation performance of the network, demonstrating a comprehensive approach to tackling the challenges posed by multi-rate SPCNs.

#### IV. NUMERICAL SIMULATION

In this section, a simulation example is presented to demonstrate the effectiveness of the employed impulsive estimator under constrained bit rates.

We consider a multi-rate SPCN with the state update period  $\hbar = 1$ , which has the following parameters:

$$\begin{aligned}
 A_1 &= \begin{bmatrix} 0.36 & 0.2 \\ 0.13 & 0.15 \end{bmatrix}, \Gamma_1 = \begin{bmatrix} 0.3 & 0.2 \\ 0.4 & 0.4 \end{bmatrix}, \\
 A_2 &= [0.31 \ 0.15]^T, A_3 = [0.83 \ 0.73], A_4 = 0.6, \\
 H_1 &= [0.16 \ 0.15 \ 0.2]^T, H_2 = [0.26 \ 0.25 \ 0.3]^T, \\
 H_3 &= [0.21 \ 0.22 \ 0.25]^T, M_1 = [0.1 \ 0.2 \ 0.2]^T, \\
 M_2 &= [0.5 \ 0.3 \ 0.2]^T, M_3 = [0.2 \ 0.3 \ 0.1]^T, \\
 \Gamma_2 &= [0.2 \ 0.3]^T, \Gamma_3 = [0.35 \ 0.46], \Gamma_4 = 0.6, \\
 W &= \begin{bmatrix} -0.3 & 0.1 & 0.2 \\ 0.1 & -0.3 & 0.2 \\ 0.1 & 0.2 & -0.3 \end{bmatrix}, C_1 = \begin{bmatrix} 0.8 & 0.1 & 0 \\ 0.2 & 1.1 & 0 \\ 0 & 0 & 1 \end{bmatrix}, \\
 C_2 &= \begin{bmatrix} 1.1 & 0 & 0 \\ 0 & 0.8 & 0 \\ 0 & 0 & 0.9 \end{bmatrix}, C_3 = \begin{bmatrix} 0.8 & 0 & 0 \\ 0 & 1 & 0 \\ 0 & 0 & 0.9 \end{bmatrix}, \\
 D &= [0.5 \ 0.5]^T, F = 2.
 \end{aligned}$$

Let the external disturbance be  $\vartheta(p_t) = 0.8 \cos(p_t)$ , which implies  $\vartheta_0 = 0.8$ . The nonlinear functions are chosen as

$$\begin{cases} \tilde{g}(x_{if}(p_t)) = 0.45 \begin{bmatrix} \tanh(0.2x_{if}^{(1)}(p_t)) \\ \tanh(0.2x_{if}^{(2)}(p_t)) \end{bmatrix} \\ \tilde{h}(x_{is}(p_t)) = 0.36(|x_{is}(p_t) + 1| - |x_{is}(p_t) - 1|) \end{cases}$$

where  $x_{if}^{(1)}(p_t)$  and  $x_{if}^{(2)}(p_t)$  represent the first and the second component of the state  $x_{if}(p_t)$ , respectively.

Let the attenuation coefficients be  $\beta_1 = 1.02, \beta_2 = 0.56$  and the SPP be  $\varepsilon \in (0, 0.07]$ . Assume that the sampling period of sensor is  $b = 2$ . The initial values of the SPCN's state are set to be

$$\begin{aligned}
 x_1(p_0) &= [0.4 \ 0.2 \ 0.1]^T, x_2(p_0) = [0.2 \ 0.2 \ 0.3]^T, \\
 x_3(p_0) &= [0.1 \ 0.1 \ 0.1]^T, \hat{x}_1(p_0) = -[0.1 \ 0.3 \ 0.2]^T, \\
 \hat{x}_2(p_0) &= [0.1 \ 0.1 \ 0.4]^T, \hat{x}_3(p_0) = -[0.3 \ 0.2 \ 0.1]^T.
 \end{aligned}$$

Based on the aforementioned parameter settings, the estimation performance of SPCNs is analyzed under impulsive estimation method and various bit rate allocation protocols.

Firstly, we employ an average allocation strategy (AAS) for computing the impulsive estimator gains. This strategy ensures that each node in the network is assigned with identical bit rates, thereby guaranteeing an equitable distribution of network resources. Assume that the available bit rates of the entire wireless network are  $B = 30$  bps. We have  $B_1 = B_2 = B_3 = \lfloor B/3 \rfloor = 10$  bps by AAS. The parameters of the uniform quantizer are given as  $\sigma_1 = 0.3, \sigma_2 = 0.5$  and

TABLE I  
EFFECT OF DIFFERENT SAMPLING PARAMETERS ON THE ERROR BOUND

Sampling period $b$	2	3	5	7	9
Bound $\sqrt{\bar{\delta}}$	2.987	3.2566	3.7324	4.1496	4.5273

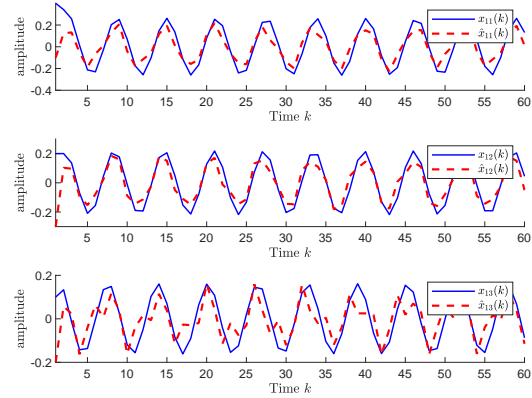


Fig. 2. State and estimation for the node 1.

$\sigma_3 = 1$ . In this example, we choose the SPP as  $\varepsilon = 0.06$ , and obtain the gains of the impulsive estimator as

$$\begin{aligned}
 L_1 &= \begin{bmatrix} 0.9118 & -0.031 & 0 \\ -0.1251 & 0.7382 & 0 \\ 0 & 0 & 0.7904 \end{bmatrix}, \\
 L_2 &= \begin{bmatrix} 0.7246 & -0.0165 & 0 \\ -0.006 & 0.8852 & 0 \\ 0 & 0 & 0.8282 \end{bmatrix}, \\
 L_3 &= \begin{bmatrix} 0.9101 & 0.0034 & 0 \\ 0.0011 & 0.7839 & 0 \\ 0 & 0 & 0.8244 \end{bmatrix}.
 \end{aligned}$$

The system states and their estimates are depicted in Figs. 2-4, where  $x_{ij}(p_t)$  denotes the  $j$ -th component of the state of node  $i$ . The error norm  $\|\tilde{e}(p_t)\|$  and the estimation error bound  $\sqrt{\bar{\delta}} = 2.987$  are plotted in Fig. 5, which verifies that the estimation error is indeed ultimately bounded.

The sampling period of sensor determines the frequency of estimator updates, hence the integer  $b$  has a significant impact on the estimation performance. Keeping the system parameters constant, we analyze the relationship between different integer  $b$  and the upper bound of estimation error, as shown in Table I. When the sensor sampling period decreases (the impulse triggering times more frequent), the bound  $\sqrt{\bar{\delta}}$  becomes smaller, indicating better system estimation performance.

Reflecting on the inequality (42), it becomes evident that the estimation error is intricately related to the allocation of bit rates to individual nodes. The AAS mentioned above serves as a conventional approach to bit rate allocation, however, it may not be the optimal allocation scheme. This is particularly true in practical scenarios where certain nodes may require higher transmission speeds to execute more complex tasks compared to others. Therefore, we employ the PSO algorithm

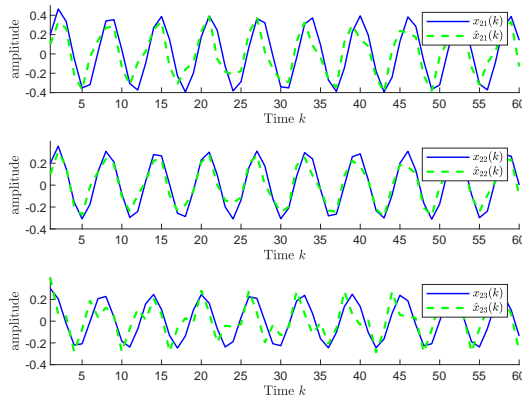


Fig. 3. State and estimation for the node 2.

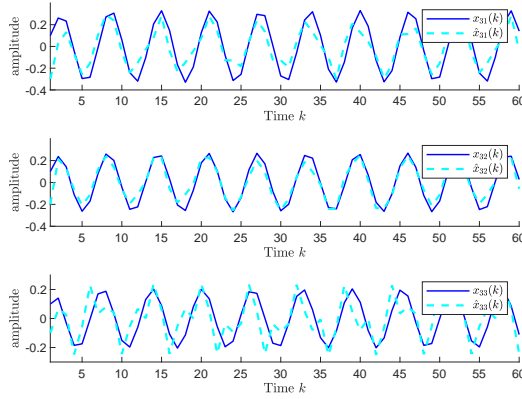


Fig. 4. State and estimation for the node 3.

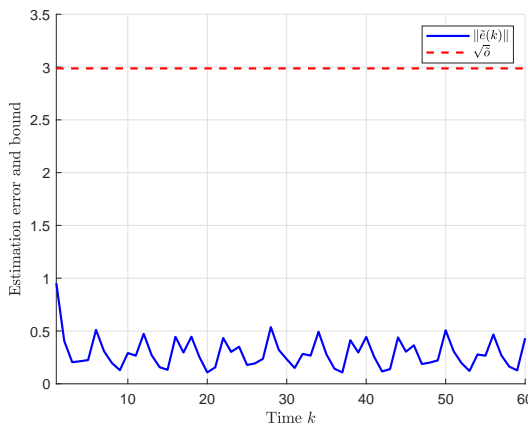


Fig. 5. Estimate error and bound.

TABLE II  
 EFFECT OF DIFFERENT PROTOCOLS ON THE ERROR BOUND

Parameters	$B$ (bps)	Protocol	Bit rate allocation	
			$B_1, B_2, B_3$ (bps)	Bound
$\sigma_1=0.3$ $\sigma_2=0.5$ $\sigma_3=0.1$	50	AAS	16, 16, 16	3.2324
	50	PSO	14, 16, 20	3.2315
	30	AAS	10, 10, 10	3.2566
	30	PSO	8, 10, 12	3.2482
	10	AAS	3, 3, 3	3.8328
	10	PSO	1, 3, 6	3.6286
$\sigma_1=1$ $\sigma_2=2$ $\sigma_3=3$	50	AAS	16, 16, 16	3.2476
	50	PSO	14, 17, 19	3.2398
	30	AAS	10, 10, 10	3.491
	30	PSO	7, 10, 13	3.4262
	10	AAS	3, 3, 3	7.4073
	10	PSO	1, 3, 6	6.5549

to dynamically adjust the bit rate allocation strategy. The superiority of the PSO-based approach over the conventional AAS becomes apparent in the subsequent analysis.

Setting  $b = 3$ , and given the quantization parameters as  $\sigma_1 = 0.3$ ,  $\sigma_2 = 0.5$  and  $\sigma_3 = 0.1$ , the error bound is obtained using both the AAS and PSO-based allocation methods in Table II. The variation of the error bound is also analyzed for a set of different quantization parameters  $\sigma_1 = 1$ ,  $\sigma_2 = 2$  and  $\sigma_3 = 3$ . The PSO algorithm is observed to not only maximize the utilization of network resources but also optimize bit rate allocation according to the specific demands of each node, thereby enhancing the estimation performance of the SPCNs. Additionally, it is inferred that an increase in available bit rates  $B$  correlates with a gradual decrease in the error bound. The quantization parameters play a crucial role in determining the decoding accuracy of the data, and a more suitable parameter setting is expected to result in an overall reduction in estimation errors.

## V. CONCLUSION

This work has addressed the ultimately bounded state estimation in multi-rate SPCN with bit rate constraints. Tailoring our approach to the multi-rate nature of the system, we have employed an impulsive method to tackle the inconsistency between the system state update period and the sensor sampling period. Utilizing the structural characteristics of SPCN and the features of the coding-decoding mechanism, an estimator with impulsive dynamics behavior has been devised. Within this framework, a sufficient condition ensuring the exponential boundedness of the estimation error dynamics has been derived. By iterating the Lyapunov functions obtained at two rates, we have established an upper bound on the error dynamics. The collaborative design of the impulsive estimator and bit rate allocation strategy has been facilitated by introducing the PSO algorithm. Finally, the effectiveness of the proposed impulsive strategy has been demonstrated, and a detailed analysis of the relationship between estimation performance and constrained bit rates has been provided.

In the future, to deal with the characteristics of the SPCNs with different time scales (e.g. fast and slow states), a differential coding process tailored to these dynamics could be

introduced, which would enable further data compression and help conserve limited bandwidth. Also, we could extend the main results of this paper to more general systems with more specific application insights [41]–[44].

## REFERENCES

- [1] R. Caballero-Águila, A. Hermoso-Carazo and J. Linares-Pérez, Networked fusion estimation with multiple uncertainties and time-correlated channel noise, *Information Fusion*, vol. 54, pp. 161-171, Feb. 2020.
- [2] W.-H. Chen, H. He, X. Lu and X. Deng, Impulsive observer-based design for state estimation of a class of nonlinear singularly perturbed systems with discrete measurements, *Nonlinear Analysis: Hybrid Systems*, vol. 41, art. no. 101027, Aug. 2021.
- [3] W.-H. Chen, Z. Ruan and W. X. Zheng, Stability and  $L_2$ -gain analysis for linear time-delay systems with delayed impulses: An augmentation-based switching impulse approach, *IEEE Transactions on Automatic Control*, vol. 64, no. 10, pp. 4209-4216, Oct. 2019.
- [4] S. Cheng, H. Li, Y. Guo, T. Pan, Y. Fan, Event-triggered optimal nonlinear systems control based on state observer and neural network, *Journal of Systems Science & Complexity*, vol. 36, no. 1, pp. 222-238, 2023.
- [5] D. Dai, J. Li, Y. Song and F. Yang, Event-based recursive filtering for nonlinear bias-corrupted systems with amplify-and-forward relays, *Systems Science & Control Engineering*, vol. 12, no. 1, art. no. 2332419, 2024.
- [6] F. Deng, Y. Ming and B. Lyu, CCE-Net: causal convolution embedding network for streaming automatic speech recognition, *International Journal of Network Dynamics and Intelligence*, vol. 3, no. 3, art. no. 100019, Sept. 2024.
- [7] M. Elsheikh, R. Hille, A. Tatulea-Codrean and S. Kramer, A comparative review of multi-rate moving horizon estimation schemes for bioprocess applications, *Computers and Chemical Engineering*, vol. 146, art. no. 107219, Mar. 2021.
- [8] C. Gao, Z. Wang, L. Ma, H. Liu and X. He, Private synchronization control of complex networks against eavesdropping attacks: A differential privacy scheme, *IEEE Transactions on Network Science and Engineering*, vol. 11, no. 3, pp. 3028-038, May 2024.
- [9] P. Gao, C. Jia and A. Zhou, Encryption-decryption-based state estimation for nonlinear complex networks subject to coupled perturbation, *Systems Science & Control Engineering*, vol. 12, no. 1, art. no. 2357796, 2024.
- [10] F. Han, J. Liu, J. Li, J. Song, M. Wang and Y. Zhang, Consensus control for multi-rate multi-agent systems with fading measurements: the dynamic event-triggered case, *Systems Science & Control Engineering*, vol. 11, no. 1, art. no. 2158959, 2023.
- [11] H. Han, S. Fu, H. Sun and J. Qiao, Data-driven multimodel predictive control for multirate sampled-data nonlinear systems, *IEEE Transactions on Automation Science and Engineering*, vol. 20, no. 3, pp. 2182-2194, Jul. 2023.
- [12] N. Hou, Z. Wang, Y. Shen, H. Liu and H. Dong, A non-fragile approach to fault estimation for a class of multi-rate systems under binary encoding schemes, *International Journal of Robust and Nonlinear Control*, vol. 34, no. 2, pp. 751-772, 2024.
- [13] Z. Huang, W. Lv, C. Liu, Y. Xu, L. Rutkowski and T. Huang, Event-triggered distributed moving horizon estimation over wireless sensor networks, *IEEE Transactions on Industrial Informatics*, vol. 20, no. 3, pp. 4218-4226, Mar. 2024.
- [14] O. Jaramillo, B. Castillo-Toledo and S. Di Gennaro, Robust impulsive observer-based stabilization for uncertain nonlinear systems with sampled-output, *IEEE Control Systems Letters*, vol. 5, no. 3, pp. 845-850, Jul. 2021.
- [15] L. Lan, G. Wei, D. Ding and J. Zhang, Zonotopic distributed fusion over binary sensor networks with bit rate allocation: A coding-decoding approach, *IEEE Transactions on Cybernetics*, vol. 54, no. 11, pp. 6855-6866, Nov. 2024.
- [16] C. Li, Y. Liu, M. Gao and L. Sheng, Fault-tolerant formation consensus control for time-varying multi-agent systems with stochastic communication protocol, *International Journal of Network Dynamics and Intelligence*, vol. 3, no. 1, art. no. 100004, Mar. 2024.
- [17] J.-Y. Li, Z. Wang, R. Lu, and Y. Xu, Distributed filtering under constrained bit rate over wireless sensor networks: Dealing with bit rate allocation protocol, *IEEE Transactions on Automatic Control*, vol. 68, no. 3, pp. 1642-1654, Mar. 2023.
- [18] T. Li, Z. Wang, L. Zou, B. Chen, L. Yu, A dynamic encryption-decryption scheme for replay attack detection in cyber-physical systems, *Automatica*, vol. 151, art. no. 110926, May 2023.
- [19] W. Li, Z. Wang, J. Hu, J. Du and W. Sheng, Kernel adaptive filtering over complex networks, *IEEE Transactions on Neural Networks and Learning Systems*, vol. 35, no. 3, pp. 4339-4346, Mar. 2024.
- [20] K. Liang, W. He, J. Xu, and F. Qian, Impulsive effects on synchronization of singularly perturbed complex networks with semi-Markov jump topologies, *IEEE Transactions on Systems, Man, and Cybernetics: Systems*, vol. 52, no. 5, pp. 3163-3173, May 2022.
- [21] Y. Liang, T. Chen and Q. Pan, Multi-rate stochastic  $H_\infty$  filtering for networked multi-sensor fusion, *Automatica*, vol. 46, no. 2, pp. 437-444, Feb. 2010.
- [22] C. Liu, H. Rao, X. Yu, Y. Xu and C.-Y. Su, State estimation for recurrent neural networks with intermittent transmission, *IEEE Transactions on Cybernetics*, vol. 54, no. 5, pp. 2891-2900, May 2024.
- [23] S. Liu, J. Cheng, H. Yan and D. Zhang, Adaptive neural sliding-mode control for fuzzy singularly perturbed systems: Sojourn-probability-based stochastic communication protocol, *IEEE Transactions on Cybernetics*, vol. 54, no. 10, pp. 6095-6104, Oct. 2024.
- [24] Y. Liu and Q. Ling, Stabilizing bit rate conditions for a scalar linear event-triggered system with Markov dropouts, *Automatica*, vol. 146, art. no. 110635, Dec. 2022.
- [25] W. Qi, C. Zhang, G. Zong, S.-F. Su and M. Chadli, Finite-time event-triggered stabilization for discrete-time fuzzy Markov jump singularly perturbed systems, *IEEE Transactions on Cybernetics*, vol. 53, no. 7, pp. 4511-4520, Jul. 2023.
- [26] H. Shen, X. Hu, X. Wu, S. He and J. Wang, Generalized dissipative state estimation of singularly perturbed switched complex dynamic networks with persistent dwell-time mechanism, *IEEE Transactions on Systems, Man, and Cybernetics: Systems*, vol. 52, no. 3, pp. 1795-1806, Mar. 2022.
- [27] L. Shi, Z. Ma, S. Yan and T. Ao, Flocking dynamics for cooperation-antagonism multi-agent networks subject to limited communication resources, *IEEE Transactions on Circuits and Systems I: Regular Papers*, vol. 71, no. 3, pp. 1396-1405, Mar. 2024.
- [28] W. Song, Z. Wang, Z. Li, J. Wang and Q.-L. Han, Nonlinear filtering with sample-based approximation under constrained communication: progress, insights and trends, *IEEE/CAA Journal of Automatica Sinica*, vol. 11, no. 7, pp. 1539-1556, Jul. 2024.
- [29] B. Sun, Ma. Fan, G. Liu, M. Lv, S. Liu, M. He, K. Huang, C. Yang, A dynamics-learning multirate estimation approach for the feeding condition perception of complex industry processes, *IEEE Transactions on Cybernetics*, vol. 54, no. 5, pp. 3286-3298, May 2024.
- [30] H. Viumdal, S. Mylvaganam and D. Di Ruscio, System identification of a non-uniformly sampled multi-rate system in aluminium electrolysis cells, *Modeling, Identification and Control*, vol. 35, no. 3, pp. 127-146, Oct. 2014.
- [31] X. Wan, Z. Wang, M. Wu and X. Liu,  $H_\infty$  state estimation for discrete-time nonlinear singularly perturbed complex networks under the round-robin protocol, *IEEE Transactions on Neural Networks and Learning Systems*, vol. 30, no. 2, pp. 415-426, Feb. 2019.
- [32] J. Wang, Z. Huang, Z. Wu, J. Cao and H. Shen, Extended dissipative control for singularly perturbed PDT switched systems and its application, *IEEE Transactions on Circuits and Systems I: Regular Papers*, vol. 67, no. 12, pp. 5281-5289, Dec. 2020.
- [33] L. Wang, Z. Wang, D. Zhao, Y. Liu and G. Wei, Recursive filtering for discrete-time stochastic complex networks under bit-rate constraints: a locally minimum variance approach, *IEEE Transactions on Automatic Control*, vol. 69, no. 5, pp. 3441-3448, May. 2024.
- [34] R. Wang, B. Chen, Z. Hu, D. W. C. Ho and L. Yu, Distributed event-triggered fusion estimation for networked asynchronous multi-rate systems, *Information Fusion*, vol. 98, art. no. 101846, Oct. 2023.
- [35] W. Wang and M. Wang, Adaptive neural event-triggered output-feedback optimal tracking control for discrete-time pure-feedback nonlinear systems, *International Journal of Network Dynamics and Intelligence*, vol. 3, no. 2, art. no. 100010, Jun. 2024.
- [36] Y. Wang, C. K. Ahn, H. Yan and S. Xie, Fuzzy control and filtering for nonlinear singularly perturbed Markov jump systems, *IEEE Transactions on Cybernetics*, vol. 51, no. 1, pp. 297-308, Jan. 2021.
- [37] Y. Wang, Z. Wang, L. Zou and H. Dong, On  $H_\infty$  fuzzy proportional-integral observer design under amplify-and-forward relays and multirate measurements, *IEEE Transactions on Fuzzy Systems*, vol. 32, no. 4, pp. 1873-1885, Apr. 2024.
- [38] Z. Xia, M. Hu, W. Dai, H. Yan and X. Ma, Q-learning-based multi-rate optimal control for process industries, *IEEE Transactions on Circuits and Systems II: Express Briefs*, vol. 70, no. 6, pp. 2006-2010, Jun. 2023.
- [39] L. Yang, W. Lv, Y. Xu, J. Tao and D. E. Quevedo, Structure-aware reinforcement learning for optimal transmission scheduling over packet length-dependent lossy networks, *IEEE Transactions on Automatic Control*, in press, DOI: 10.1109/TAC.2024.3488823.
- [40] L. Yang, Y. Xu, W. Lv, J.-Y. Li and L. Shi, Optimal transmission scheduling over multi-hop networks: Structural results and reinforcement learning, *IEEE Transactions on Automatic Control*, vol. 69, no. 3, pp. 1826-1833, Mar. 2024.

- [41] X. Yi and T. Xu, Distributed event-triggered estimation for dynamic average consensus: A perturbation-injected privacy-preservation scheme, *Information Fusion*, vol. 108, art. no. 102396, Aug. 2024.
- [42] X. Yi, Z. Wang, S. Liu and Q. Tang, Acceleration model considering multi-stress coupling effect and reliability modeling method based on nonlinear Wiener process, *Quality and Reliability Engineering International*, vol. 40, no. 6, pp. 3055-3078, May. 2024.
- [43] X. Yi, H. Yu and T. Xu, Solving multi-objective weapon-target assignment considering reliability by improved MOEA/D-AM2M, *Neurocomputing*, vol. 563, art. no. 126906, Jan. 2024.
- [44] X. Yi, C. Xu, X. Fang and S. Liu, A new reliability analysis method for software-intensive systems with degradation accumulation effect based on goal oriented methodology, *Quality and Reliability Engineering International*, vol. 40, no. 1, pp. 236-260, May. 2023.
- [45] M. Yuan and W. Qian, Adaptive output feedback tracking control for nonlinear systems with unknown growth rate, *International Journal of Network Dynamics and Intelligence*, vol. 3, no. 1, art. no. 100002, Mar. 2024.
- [46] D. Zhang, Q.-G. Wang, D. Srinivasan, H. Li and L. Yu, Asynchronous state estimation for discrete-time switched complex networks with communication constraints, *IEEE Transactions on Neural Networks and Learning Systems*, vol. 29, no. 5 pp. 1732-1746, May 2018.
- [47] W. Zhang, L. Sheng and M. Gao, Finite-horizon  $H_\infty$  state estimation for time-varying complex networks based on the outputs of partial nodes, *Systems Science & Control Engineering*, vol. 9, no. s2, pp. 48-59, May 2021.
- [48] L. Zhao and B. Li, Adaptive fixed-time control for multiple switched coupled neural networks, *International Journal of Network Dynamics and Intelligence*, vol. 3, no. 3, art. no. 100018, Sept. 2024.
- [49] X. Zhao and S. Liu, Distributed recursive filtering for multi-rate nonlinear systems under the round-robin scheduling, *Nonlinear Dynamics*, vol. 107, pp. 939-952, Jan. 2022.
- [50] Z. Zhao, Z. Wang and L. Zou, Sequential fusion estimation for multirate complex networks with uniform quantization: a zonotopic set-membership approach, *IEEE Transactions on Neural Networks and Learning Systems*, vol. 35, no. 4, pp. 5764-5777, Apr. 2024.
- [51] S. Zhu, J. Zhou, X. Yu and J. Lu, Bounded synchronization of heterogeneous complex dynamical networks: a unified approach, *IEEE Transactions on Automatic Control*, vol. 66, no. 4, pp. 1756-1762, Apr. 2021.
- [52] L. Zou, Z. Wang, B. Shen and H. Dong, Encryption-decryption-based state estimation with multirate measurements against eavesdroppers: a recursive minimum-variance approach, *IEEE Transactions on Automatic Control*, vol. 68, no. 12, pp. 8111-8118, Dec. 2023.



**Yuru Guo** was born in Hubei province, China, in 1997. She received her B.S. degree from the school of electrical engineering, Nanjing Institute of Technology, Jiangsu, China, in 2019, majoring in Building Electricity and Intelligence. She is currently working toward the Ph.D. degree in Control Science and Engineering at Guangdong University of Technology, Guangzhou, China.

She was a Visiting Ph.D. student with the Department of Computer Science, Brunel University London, Uxbridge, U.K., from 2023 to 2024. Her

research interests include networked control systems and impulsive control.



**Zidong Wang** (Fellow, IEEE) received the B.Sc. degree in mathematics in 1986 from Suzhou University, Suzhou, China, and the M.Sc. degree in applied mathematics in 1990 and the Ph.D. degree in electrical engineering in 1994, both from Nanjing University of Science and Technology, Nanjing, China.

He is currently a Professor of Dynamical Systems and Computing in the Department of Computer Science, Brunel University London, U.K. From 1990 to 2002, he held teaching and research appointments in universities in China, Germany and the U.K. Prof. Wang's research interests include dynamical systems, signal processing, bioinformatics, control theory and applications. He has published a number of papers in international journals. He is a holder of the Alexander von Humboldt Research Fellowship of Germany, the JSPS Research Fellowship of Japan, William Mong Visiting Research Fellowship of Hong Kong.

Prof. Wang serves (or has served) as the Editor-in-Chief for *International Journal of Systems Science*, the Editor-in-Chief for *Neurocomputing*, the Editor-in-Chief for *Systems Science & Control Engineering*, and an Associate Editor for 12 international journals including *IEEE Transactions on Automatic Control*, *IEEE Transactions on Control Systems Technology*, *IEEE Transactions on Neural Networks*, *IEEE Transactions on Signal Processing*, and *IEEE Transactions on Systems, Man, and Cybernetics-Part C*. He is a Member of the Academia Europaea, a Member of the European Academy of Sciences and Arts, an Academician of the International Academy for Systems and Cybernetic Sciences, a Fellow of the IEEE, a Fellow of the Royal Statistical Society and a member of program committee for many international conferences.



**Jun-Yi Li** (Member, IEEE) was born in Henan province, China, in 1991. He received the M.S. degree in control science and engineering from Hangzhou Dianzi University, Hangzhou, China, in 2017 and the Ph.D. degree in Control Science and Engineering from Guangdong University of Technology, Guangzhou, China, in 2021. He is currently a Lecturer with the School of Automation, Guangdong University of Technology, and also with the Project Team of Intelligent Unmanned Surface Vessels for Waste Collection, Pazhou Lab, Guangzhou.

He was a visiting Ph.D. student with the Department of Computer Science, Brunel University London, Uxbridge, U.K., from October 2019 to October 2020. His research interests include complex dynamical networks, networked systems.



**Yong Xu** (Member, IEEE) was born in Zhejiang Province, China, in 1983. He received the B.S. degree in information engineering from Nanchang Hangkong University, Nanchang, China, in 2007, the M.S. degree in control science and engineering from Hangzhou Dianzi University, Hangzhou, China, in 2010, and the Ph.D. degree in control science and engineering from Zhejiang University, Hangzhou, China, in 2014. He was a visiting internship student with the department of Electronic and Computer Engineering, Hong Kong University of Science and Technology, Hong Kong, China, from June 2013 to November 2013, where he was a Research Fellow from February 2018 to August 2018. Now he is a professor with School of Automation, at Guangdong University of Technology, Guangzhou, China.

His research interests include PID control, networked control systems, state estimation, and positive systems.